PERFORMANCE ENHANCEMENTS OF RANGING RADIO AIDED NAVIGATION

THESIS

PATRIC J. ERNSBERGER, Maj, USAF

AFIT/GE/ENG/09-15

DEPARTMENT OF THE AIR FORCE
AIR UNIVERSITY

AIR FORCE INSTITUTE OF TECHNOLOGY

Wright-Patterson Air Force Base, Ohio

AFIT/GE/ENG/09-15

Performance Enhancements of Ranging Radio Aided Navigation

THESIS

Presented to the Faculty

Department of Electrical and Computer Engineering

Graduate School of Engineering and Management

Air Force Institute of Technology

Air University

Air Education and Training Command

In Partial Fulfillment of the Requirements for the

Degree of Master of Science in Electrical Engineering
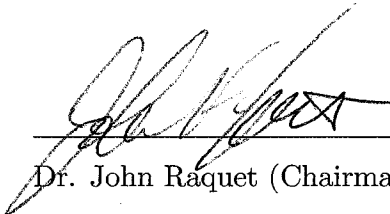
PATRIC J. ERNSBERGER, B.S.

Maj, USAF

March 2009

Performance Enhancements of Ranging Radio Aided Navigation

PATRIC J. ERNSBERGER, B.S.

Maj, USAF

Approved:

_____   _____
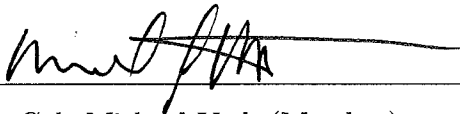Dr. John Raquet (Chairman)   18 MAR 09
                                        Date

_____   _____
Lt Col. Michael Veth (Member)   18 MAR 09
                                        Date

_____   _____
Dr. Meir Pachter (Member)   18.3.09
                                        Date

AFIT/GE/ENG/09-15

Abstract

Determining the position of team member's is always useful information, whether it is a team of fire fighters fighting a blaze or combatants clearing a building in the field. This information becomes even more decisive for the people responsible for their safety. To accomplish this in areas denied Global Navigation Satellite System (GNSS), such as around buildings or in steep valleys, alternative methods must be used. Radio ranging systems have been a part of the navigation solution for years. They unfortunately have poor performance in certain areas, such as inside buildings, due to multipath and other errors. To improve the position estimate it is believed that using vision, consumer grade inertial navigation systems, and any other measurement available can aid the navigation solution. To accomplish this, an extended Kalman filter was developed. It was configured as a centralized filter. This produced a baseline, showing that as image measurements were added, the navigation solution did improve. To simulate this with multiple vehicles and/or soldiers required a large state vector for the Kalman filter. To manage the large number of states and efficiently incorporate them into influence matrices, a "Rosetta stone" was designed for state management. This "Rosetta stone" breaks the states into simpler blocks such as position and attitude for the soldier and position for the image features. This in turn made updating the influence matrix and covariance matrix a smoother process. The impact of adding image measurements has been two fold. First, the position RMS errors were reduced by approximately a factor of 2. Second, the attitude which fluctuated greatly in the radio only cases was reduced by a factor of 10 through image aiding.

Table of Contents

List of Figures

List of Tables

Performance Enhancements of Ranging Radio Aided Navigation

I. Introduction

This document's purpose is to describe the research in the application of multi vehicle radio ranging and the benefit of adding imaging to its navigation solution. The need to ensure precision navigation in locations where Global Navigation Satellite Systems (GNSS) do not work has become increasingly valuable. Since the 1991 Gulf War, precision navigation has been crucial to miliary actions [8]. This research is one facet of the research being accomplished to reduce the reliance placed on GNSS. The use of radio ranging in positioning has been used for years [7]. It however has limitations when used as a stand-alone solution. Starting with geometry, generally in a scenario were soldiers are maneuvering on the ground, there is rarely significant differences in height of the soldiers thus reducing the accuracy of the height solution. Radio systems used in urban environment also have difficulties with multipath as the soldiers move through the building. There can also be significant clock errors from the need to keep all the radios synchronized in time. These errors can be reduced with the aid of vision measurements and inertial measurements.

1.1 Problem Statement

The goal of this research is to develop the ability to simulate multiple vehicles that can incorporate combinations of different measurements to specifically: radio inter-vehicle ranging, fixed radio ranging, imaging, and barometer-altimeter measurements. The primary objective is to determine the overall performance impacts of the different measurements together, with particular emphasis on the benefits of adding vision/inertial measurements to a radio ranging based system.

1.2 Assumptions

The first assumption is that the image ranging will be accomplished using a single camera. One approach for this is using coded aperture which is currently being developed at the Air Force Institute of Technology (AFIT) [3] and for the purposes of this research will be assumed to be viable. This scenario also assumes that there is no limit on the communications bandwidth for the radio. This allows unlimited amounts of data to be transmitted between soldiers supporting later assumptions. It is also assumed that the there is no measurement delay which would not be true for live systems. It is also assumed that the measurements are available at the central processing mode so all the measurements are available for the centralized extended Kalman filter.

1.3 Methodology

To document the research conducted in this thesis, each chapter will be briefly summarized. The first chapter is an overview of research conducted specifically in the area of incorporating multi-vehicle with multiple measurement types. The second chapter is the background for the research. This includes basic navigation overview to include frames of reference and the methods to go between frames. A brief synopsis of imaging is included. Kalman filtering and extended Kalman filtering is briefly examined. Chapter three is work unique to this research. This begins with the design of the extended Kalman filter used in the research and the means of incorporating multiple vehicles. Chapter four consists of simulations and the results will describe the different test scenarios and discuss the results from them. Finally, chapter five will be the conclusion and recommendations. It will be a synopsis of the results and other work that can be done to move this research forward.

II. Navigation Mathematics Background

2.1 Coordinate Frames

The World Geodetic System 1984 (WGS 84) is a common three dimensional coordinate system. The system's defining properties is that it is geocentric (center of mass is defined for the Earth). The orientation was initially given by the Bureau International de l'Heure (BIH) of 1984. WGS 84 is a right-handed Earth-fixed orthogonal system all of which is fully described in [6].

To accomplish navigation, reference frames must be defined in order to determine position. To define reference frames in this paper [7] and [8] were used.

- Earth-fixed inertial frame (i-frame) Figure 2.1: origin is defined at the earth's center of mass, with axes that are non-rotating with respect to fixed stars (i.e., first star of Aries).

- Earth-centered Earth-fixed frame (e-frame) Figure 2.1: origin is at the Earth's center of mass, with axes fixed to and rotating, with the earth. Its axes are z along the Earth's polar axis through the north pole, x is in the equatorial plane through Greenwich meridian, and y is also on the equatorial plane 90 degrees east in longitude from x.

- Vehicle fixed navigation frame (n'-frame) Figure 2.1: origin is at the center of gravity of the vehicle or another point on the vehicle. The axes are north, east and down (NED) from the origin.

- Earth fixed navigation frame (n-frame) Figure 2.1: has an origin at some pre-defined location on Earth, and its axes x, y, and z are in the NED direction as in the vehicle fixed navigation frame.

- Body frame (b-frame): origin is the same as the vehicle fixed navigation frame, and typically its axes x, y, and z are out the nose, right wing, and bottom of
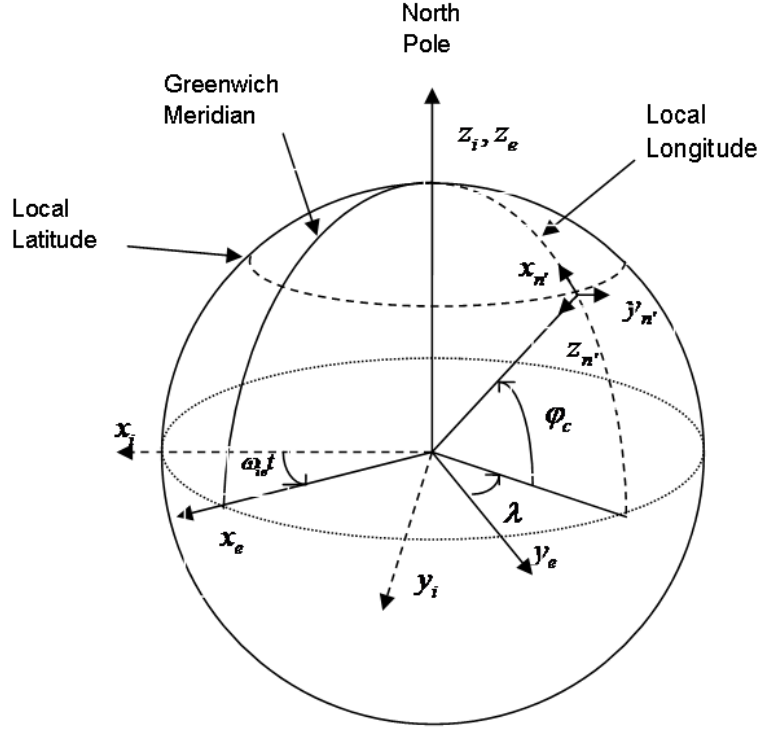
Figure 2.1: Earth with the i-frame, e-frame, and n'-frames [8]

an aircraft. For this research, the axis x, y, and z axes are out the nose of the troop, the right shoulder, and down through the soldier's body.

- Camera frame (c-frame): origin is at the camera's optical center. The camera frame x and y are up and to the right of the optical center. The z axes is out of the plane defined by x and y along the direction the camera is pointed.

2.2   Coordinate Frames Transforms

The ability to move between different coordinate reference frames is extremely important in navigation. Using [7] and [8] the relevant transforms will be developed.

Coordinate frame transforms allow vectors to be converted from one frame of reference to another, and this is normally accomplished using a Direction Cosine Matrix (DCM). DCM is expressed as a 3×3 matrix which is the inner product of the unit basis vector in one frame with each of the unit basis vectors in another frame.

The elements of the DCM are broken into the ith row and jth column each representing the cosine of the i-axis of the a-frame and the j-axis of the b-frame.

$$\mathbf{C}_a^b = \begin{bmatrix} c_{11} & c_{12} & c_{13} \\ c_{21} & c_{22} & c_{23} \\ c_{31} & c_{32} & c_{33} \end{bmatrix} \tag{2.1}$$

$$p^b = \mathbf{C}_a^b p^a \tag{2.2}$$

The DCM has the following properties if used with a right hand Cartesian frame:

1. $Det(\mathbf{C}_a^b) \equiv \left| \mathbf{C}_a^b \right| = 1$
2. $\mathbf{C}_a^b = \left(\mathbf{C}_a^b \right)^{-1} = \left(\mathbf{C}_a^b \right)^T$
3. $\mathbf{C}_a^c = \mathbf{C}_b^c \mathbf{C}_a^b$

The Earth frame to navigation frame (north, east, down) transformation is

$$\mathbf{C}_e^{n'} = \begin{bmatrix} -\sin \mathbf{L} \cos \boldsymbol{\lambda} & -\sin \mathbf{L} \sin \boldsymbol{\lambda} & \cos \mathbf{L} \\ -\sin \boldsymbol{\lambda} & \cos \boldsymbol{\lambda} & \mathbf{0} \\ -\cos \mathbf{L} \cos \boldsymbol{\lambda} & -\cos \mathbf{L} \sin \boldsymbol{\lambda} & -\sin \boldsymbol{\lambda} \end{bmatrix} \tag{2.3}$$

Where L is the latitude and λ longitude the navigation frame to the body frame DCM is given by Equation (2.4).

$$\mathbf{C}_{n'}^{b} = \begin{bmatrix} \cos\psi\cos\theta & \sin\psi\cos\theta & -\sin\theta \\ -\sin\psi\cos\phi + \cos\psi\sin\theta\sin\phi & \cos\psi\cos\phi + \sin\psi\sin\theta\sin\phi & \cos\theta\sin\phi \\ \sin\psi\sin\phi + \cos\psi\sin\theta\cos\phi & -\cos\psi\sin\phi + \sin\psi\sin\theta\cos\phi & \cos\theta\cos\phi \end{bmatrix}$$

$$(2.4)$$

Where the Euler angles are represented by ϕ as roll, θ as pitch, and ψ as yaw.

2.3 Basic Inertial Navigation

This section closely follows a similar development given in [7]. To perform inertial navigation requires a determination of angular motion through gyroscopic sensors, force measurements using accelerometers, the ability to determine force measurement into the reference frame using the attitude information given by the gyroscopes, the ability to resolve the Earth's gravitational force, and the ability to integrate the aforementioned data to find velocities and position.

Gyroscopes can be used to find the angle turned or the angular rate about an axis. There are many types of gyroscopes from the common spinning mass gyroscopes to the gas rate gyroscope [7]. The spinning mass gyroscope reacts to a tilt by moving orthogonally to the direction of the tilt and then allows angle moved to be measured. There are three reasons a gyroscope works: inertia, angular momentum, and precession. Inertia is important because it defines the direction that is fixed in the inertial reference frame. Angular momentum is the product of the inertia and the angular velocity about the same axis of rotation.

Angular momentum is defined as the ability to continue to rotate about a point unless acted upon by an external torque. It is important to consider the angular momentum of the gyroscope as this will have a great effect on the drift that the gyroscope will experience. Precession is important in the accurate measurement of angular rotation.

In this research micro-machined electromechanical system (MEMS) sensors are used. MEMS gyroscopes use Coriolis acceleration interaction on proof masses. These rely on the force interacting with the mass causing vibrations in the unit's reference frame. The Coriolis force and linear motion force result in a force perpendicular to both allowing the rotation to be measured [7].

Accelerometers are the next important component in inertial navigation; however, it must be pointed out that accelerometers measure specific force, which is the combination of acceleration and gravity effects.

An accelerometer can be simply modeled as a known mass attached to a spring allowing force to be determined on the axes of the accelerometer. When operating around the Earth gravity must also be accounted for.

The only way to account for gravity is to use a model like WGS 84 that has an approximation for gravity everywhere on Earth. With this data gravity can be properly removed from the accelerometer.

MEMS accelerometers are put into two groups [7]:

- One with a proof mass on a hinge with a mechanical sensor to detect the applied acceleration.

- The other uses a vibrating element that is measured for change in frequency of the element as tension changes with the application of force.

The information from the accelerometer then needs to be resolved into the proper frame of reference. This is accomplished by rotating the measurement from the body frame to the navigation frame using a direction cosine matrix (DCM) which is continuously updated by the gyroscope measurements.

2.4 Error Models

The error model for physical was developed using [5] and [8]. This model is based on a Taylor series approximation of the nominal solution in the nonlinear differential equation.

$$\dot{\mathbf{x}} = \mathbf{f}[\mathbf{x}(t), \mathbf{u}(t), t] \tag{2.5}$$

With $\mathbf{x}(t)$ representing the system state and $\mathbf{u}(t)$ the control input.

Perturbation about the nominal can be expressed as

$$\dot{\mathbf{x}} = \mathbf{f}[\mathbf{x}_0(t), \mathbf{u}_0(t), t] + \mathbf{F}(t)\{\mathbf{x}(t) - \mathbf{x}_0(t)\} + \mathbf{B}(t)\{\mathbf{u}(t) - \mathbf{u}_0(t)\} + \cdots \tag{2.6}$$

$$\mathbf{F}(t) = \frac{\partial \mathbf{f}}{\partial \mathbf{x}}|_{\mathbf{x}_0(t), \mathbf{u}_0(t), t} \begin{bmatrix} \frac{\partial f_1}{\partial x_1} & \cdots & \frac{\partial f_1}{\partial x_n} \\ \vdots & \ddots & \vdots \\ \frac{\partial f_n}{\partial x_1} & \cdots & \frac{\partial f_n}{\partial x_n} \end{bmatrix}_{\mathbf{x}_0(t), \mathbf{u}_0(t), t} \tag{2.7}$$

$$\mathbf{B}(t) = \frac{\partial \mathbf{f}}{\partial \mathbf{u}}|_{\mathbf{x}_0(t), \mathbf{u}_0(t), t} \begin{bmatrix} \frac{\partial f_1}{\partial u_1} & \cdots & \frac{\partial f_1}{\partial u_r} \\ \vdots & \ddots & \vdots \\ \frac{\partial f_n}{\partial u_1} & \cdots & \frac{\partial f_n}{\partial u_r} \end{bmatrix}_{\mathbf{x}_0(t), \mathbf{u}_0(t), t} \tag{2.8}$$

Neglecting higher order terms, an approximation of the differential equation or the linearized perturbation equation can then be found as

$$\dot{\mathbf{x}} = \mathbf{F}\mathbf{x} + \mathbf{B}\mathbf{u} \tag{2.9}$$

Uncertainty can be added to make this a stochastic differential equation

$$\dot{\mathbf{x}} = \mathbf{Fx} + \mathbf{Bu} + \mathbf{Gw} \qquad (2.10)$$

$$\mathbf{Q} = E[w(t)w^T(t+\tau)]\delta(\tau) \qquad (2.11)$$

The solution to this differential equation is then represented as [5]

$$\mathbf{x} = \boldsymbol{\Phi}\left(t, t_0\right)\mathbf{x}\left(t_0\right) + \int_{t_0}^{t} \boldsymbol{\Phi}\left(t, \tau\right)\mathbf{B}\left(\tau\right)\mathbf{u}\left(\tau\right)d\tau + \int_{t_0}^{t} \boldsymbol{\Phi}\left(t, \tau\right)\mathbf{G}\left(\tau\right)\mathbf{w}\left(\tau\right)d\tau \quad (2.12)$$

Where $\boldsymbol{\Phi}\left(t, t_0\right)$ is the state transition matrix from t_0 to t.

2.5 Inertial error model

The inertial navigation system navigation error model will be created based on [5], [8], and [2].

To begin with, the inertial senor will be modeled. The accelerometers and gyroscopes are modeled using a first order Gauss-Markov process and the random noise is modeled as a white Gaussian process [8]. The accelerometer is modeled as

$$\mathbf{f}_m^b = \mathbf{f}^b + \mathbf{a}^b + \mathbf{w}_a^b \qquad (2.13)$$

Where $\mathbf{f}^b$ is the true specific force, $\mathbf{a}^b$ is the accelerometer bias and $\mathbf{w}_a^b$ is the white Gaussian noise (all in the body frame).

In a similar manner, the gyroscope is modeled as

$$\boldsymbol{\omega}_m^b = \boldsymbol{\omega}^b + \mathbf{b}^b + \mathbf{w}_b^b \qquad (2.14)$$

Where $\boldsymbol{\omega}^b$ is the true angular rate, $\mathbf{b}^b$ is the gyroscope bias, and $\mathbf{w}_b^b$ is the white Gaussian noise (all in the body frame).

The first order Gauss-Markov terms $\mathbf{a}^b$ and $\mathbf{b}^b$ are modeled as

$$\dot{\mathbf{a}}^b = -\frac{1}{\tau_a}\mathbf{a}^b + \mathbf{w}^b_{a_{bias}} \qquad (2.15)$$

$$\dot{\mathbf{b}}^b = -\frac{1}{\tau_b}\mathbf{b}^b + \mathbf{w}^b_{b_{bias}} \qquad (2.16)$$

Where τ_a is the time constant for the accelerometer and τ_b is the time constant of the gyroscope and $\mathbf{w}^b_{a_{bias}}$ and $\mathbf{w}^b_{b_{bias}}$ represent the white Gaussian driving noise for the accelerometer and gyroscope.

Next, the attitude errors are modeled in the navigation frame about the NED frame.

$\boldsymbol{\psi} = [\boldsymbol{\epsilon}_n \ \boldsymbol{\epsilon}_e \ \boldsymbol{\epsilon}_d]^T$ where $\boldsymbol{\epsilon}_n, \ \boldsymbol{\epsilon}_e,$ and $\boldsymbol{\epsilon}_d$ represent the (small) angular attitude errors about the NED axis. The dynamics model of these angular errors is given as [8]

$$\dot{\boldsymbol{\psi}} = -\left[(\mathbf{C}^n_e \boldsymbol{\omega}^e_{ie}) \times\right] \boldsymbol{\psi} - \mathbf{C}^n_b \mathbf{b}^b - \mathbf{C}^n_b \mathbf{w}^b_b \qquad (2.17)$$

where $\boldsymbol{\omega}^e_{ie}$ is the earths sidereal angular rate.

Next the position and velocity errors are represented as

$$\delta \mathbf{p}^n = \tilde{\mathbf{p}}^n - \mathbf{p}^n \qquad (2.18)$$

$$\delta \mathbf{v}^n = \tilde{\mathbf{v}}^n - \mathbf{v}^n \qquad (2.19)$$

where $\tilde{\mathbf{p}}^n$ is the estimated position vector and $\mathbf{p}^n$ is the true position vector.

The velocity error dynamics are described as [8]

$$\delta \dot{\mathbf{v}}^n = \mathbf{C}^n_e \mathbf{G} \mathbf{C}^e_n \delta \mathbf{p}^n - 2\mathbf{C}^n_e \boldsymbol{\Omega}^e_{ie} \mathbf{C}^e_n \delta \mathbf{v} + (\mathbf{f}^n \times) \boldsymbol{\psi} + \mathbf{C}^n_b \mathbf{a}^b + \mathbf{C}^n_b \mathbf{w}^b_a \qquad (2.20)$$

where $\mathbf{G}$ represents the gradient of the gravity vector [8], and $\mathbf{\Omega}_{ie}^{e}$ is a skew-symmetric matrix representing the Earth's rotation rate coordinatized in the e-frame.

$$\delta\dot{\mathbf{p}}^n = \boldsymbol{\delta}\mathbf{v}^n \tag{2.21}$$

2.6 Imaging

An optical sensor is used to collect light (possibly other frequencies) and determine the strengths [8]. An optical sensor is capable of creating a multi dimensional measurement.

Digital optical sensors are made up of the following components: lens, aperture, and sensor. The lens focuses the light on the sensor and the amount of radiation is controlled by the aperture. This focused light creates the image. The image is then sampled or digitalized by the sensor.

A camera can be modeled as a pin hole where all light must pass through the origin and is inverted. The image must now be represented in terms of pixels with the origin in the upper left hand side, as seen in Figure 2.2.

The translation between the vector from the camera to the feature of interest (s^c) and pixel coordinates (s^{pix}) is accomplished by [8].

$$s^{pix} = \frac{1}{s_z^c} \begin{bmatrix} -\frac{M}{H} & 0 & \frac{M+1}{2} \\ 0 & \frac{N}{W} & \frac{N+1}{2} \\ 0 & 0 & 1 \end{bmatrix} s^c \tag{2.22}$$

or

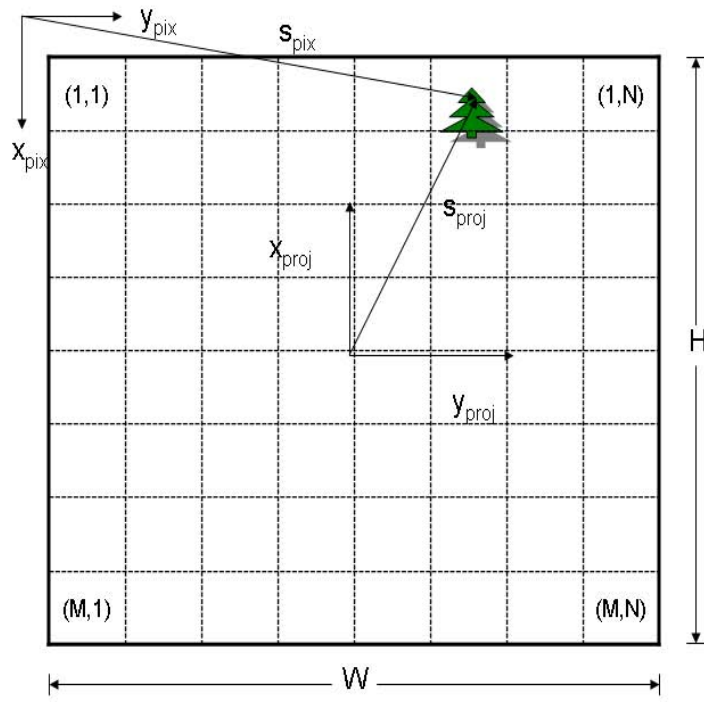$$s^{pix} = \frac{1}{s_z^c} T_c^{pix} s^c \tag{2.23}$$

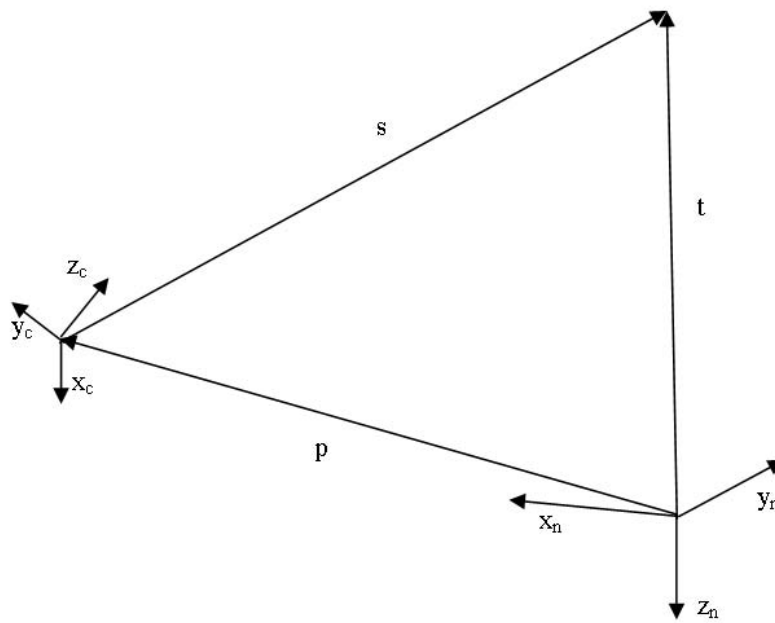Figure 2.2: This Figure is the camera pixel description from [8]

Figure 2.3: This figure shows the difference between the camera and the soldier's position in the n-frame [8].

The target location Figure 2.3 in n-frame can be obtained and the pixel coordinates can be found using the navigation state.

$$s^n = t^n - p^n \tag{2.24}$$

$$s^c = \mathbf{C}_b^c \mathbf{C}_n^b s^n \tag{2.25}$$

In the application of real lenses there are many issues that arise and must be accounted for to eliminate unwanted errors. For example, optical distortions are curvatures of straight lines at the edges of the image that can be accounted for by reducing issues with features on the edge of the field of view.

2.7 Kalman filter

2.7.1 Linear Kalman filter. Using [5], [4], and [8] the Linear Kalman filter (KF) will now be developed. The linear Kalman filter is based upon a linear system driven by white noise with deterministic inputs.

$$\dot{\mathbf{x}} = \mathbf{F}\mathbf{x} + \mathbf{B}\mathbf{u} + \mathbf{G}\mathbf{w} \tag{2.26}$$

Where $\mathbf{x}$ is the state vector, $\mathbf{F}$ is the system dynamics matrix, $\mathbf{B}$ is the input matrix $\mathbf{u}$ is the input vector, $\mathbf{G}$ is the noise matrix, and $\mathbf{w}$ is the white noise vector with noise strength of

$$\mathbf{Q}(t) = E\left[\mathbf{w}(t)\mathbf{w}^T(t+\tau)\right]\boldsymbol{\delta}(\tau) \tag{2.27}$$

The discrete-time measurement is

$$\mathbf{z}\left(t_i\right) = \mathbf{H}(t_i)\mathbf{x}(t_i) + \mathbf{v}(t_i) \tag{2.28}$$

Where $\mathbf{v}\left(t_i\right)$ is zero mean white Gaussian noise described by the covariance matrix.

$$\mathbf{R}\left(t_i\right) = \mathbf{E}\left[\mathbf{v}\left(t_i\right)\ \mathbf{v}^T\left(t_i\right)\right] \tag{2.29}$$

The KF measurement update incorporates the measurement by

$$\mathbf{K}\left(t_i\right) = \mathbf{P}(t_i^-)\mathbf{H}^T(t_i)\left[\mathbf{H}(t_i)\mathbf{P}\left(t_i^-\right)\mathbf{H}^T(t_i) + \mathbf{R}\left(t_i\right)\right]^{-1} \tag{2.30}$$

$$\hat{\mathbf{x}}(t_i^+) = \hat{\mathbf{x}}(t_i^-) + \mathbf{K}(t_i)\left[\mathbf{z}\left(t_i\right) - \mathbf{H}\hat{\mathbf{x}}(t_i^-)\right] \tag{2.31}$$

$$\mathbf{P}(t_i^+) = \mathbf{P}(t_i^-) + \mathbf{K}(t_i)\mathbf{H}(t)\mathbf{P}\left(t_i^-\right) \tag{2.32}$$

The state estimate and covariance are now propagated forward in time by

$$\dot{\hat{\mathbf{x}}}(t/t_{i-1}) = \mathbf{F}(t)\hat{\mathbf{x}}(t/t_{i-1}) + \mathbf{B}(t)\mathbf{u}(t) \tag{2.33}$$

where (t/t_{i-1}) is for any $t \ \epsilon\left[t_{i-1}, t_i\right)$ [5].

$$\dot{\mathbf{P}}(t/t_{i-1}) = \mathbf{F}(t)\mathbf{P}(t/t_{i-1}) + \mathbf{P}(t/t_{i-1})\mathbf{F}^T(t)\mathbf{G}(t)\mathbf{Q}(t)\mathbf{G}^T\left(t\right) \tag{2.34}$$

2.7.2 Extended Kalman filter. The real world unfortunately is often not linear, and as such requires a nonlinear method or linearized Kalman filter, such as the Extended Kalman Filter (EKF). Using [4] the EKF will be developed. First the systems must be defined by its now nonlinear dynamics model.

$$\dot{\mathbf{x}}(t) = \mathbf{f}\left[\mathbf{x}\left(t\right), \mathbf{u}\left(t\right), t\right] + \mathbf{G}\left(t\right)\mathbf{w}\left(t\right) \tag{2.35}$$

The nonlinear discrete time measurement is

$$\mathbf{z}(t_i) = \mathbf{h}\mathbf{x}(t_i) + \mathbf{v}(t_i) \tag{2.36}$$

Where $\mathbf{v}\left(t_i\right)$ is zero mean white Gaussian noise with strength $\mathbf{R}(t_i)$.

The EKF measurement update incorporates the measurement by

$$\mathbf{K}\left(t_i\right) = \mathbf{P}(t_i^-)\mathbf{H}^T\left[t_i; \hat{\mathbf{x}}\left(t_i^-\right)\right]\left\{\mathbf{H}\left[t_i; \hat{\mathbf{x}}\left(t_i^-\right)\right]\mathbf{P}\left(t_i^-\right)\mathbf{H}^T\left[t_i; \hat{\mathbf{x}}\left(t_i^-\right)\right] + \mathbf{R}\left(t_i^-\right)\right\}^{-1} \tag{2.37}$$

$$\hat{\mathbf{x}}(t_i^+) = \hat{\mathbf{x}}(t_i^-) + \mathbf{K}(t_i)\left\{\mathbf{z}\left(t_i\right) - \mathbf{h}\left[\hat{\mathbf{x}}(t_i^-), t_i\right]\right\} \tag{2.38}$$

$$\mathbf{P}(t_i^+) = \mathbf{P}(t_i^-) - \mathbf{K}(t_i)\mathbf{H}\left[t_i, \hat{\mathbf{x}}(t_i^-)\right]\mathbf{P}\left(t_i^-\right) \tag{2.39}$$

Where $\mathbf{H}\left[t_i; \hat{\mathbf{x}}(t_i^-)\right]$ is the partial derivative matrix which linearizes $\mathbf{h}$ about the nominal trajectory:

$$\mathbf{H}\left[t_i; \hat{\mathbf{x}}(t_i^-)\right] \triangleq \frac{\partial \mathbf{h}\left[\mathbf{x}, t_i\right]}{\partial \mathbf{x}}\big|_{\mathbf{x}=\hat{\mathbf{x}}(t/t_i)} \tag{2.40}$$

As before, the estimate is propagated forward by

$$\dot{\hat{\mathbf{x}}}(t/t_i) = \mathbf{f}\left[\hat{\mathbf{x}}(t/t_i), \mathbf{u}(t), t\right] \tag{2.41}$$

$$\dot{\mathbf{P}}(t/t_i) = \mathbf{F}\left[t; \hat{\mathbf{x}}(t/t_i)\right]\mathbf{P}(t/t_i) + \mathbf{P}(t/t_i)\mathbf{F}^T\left[t; \hat{\mathbf{x}}(t/t_i)\right] + \mathbf{G}(t)\mathbf{Q}(t)\mathbf{G}^T\left(t\right) \tag{2.42}$$

Where $\mathbf{F}\left[t;\hat{\mathbf{x}}(t/t_i)\right]$ is the partial derivative matrix which linearizes $\mathbf{f}$ about the nominal trajectory.

$$\mathbf{F}\left[t;\hat{\mathbf{x}}(t_i)\right] \triangleq \frac{\partial \mathbf{f}\left[\mathbf{x},\mathbf{u}\left(t\right),t\right]}{\partial \mathbf{x}}|_{\mathbf{x}=\hat{\mathbf{x}}(t/t_i)} \tag{2.43}$$

This chapter has reviewed briefly a wide variety of important aspects of navigation. From MEMS to the Kalman equations. All of these concepts will be put to use in Chapter 3 as the multi vehicle filter is developed.

III. Ranging and Image Multi-Vehicle Navigation algorithms

This chapter will be used to show how the centralized Kalman filter was developed to produce the optimal estimate of the current navigation state for multiple vehicles.

First, the variables will be broken down and the method that was used to track all the variables will be explained. This is important because tracking multiple vehicle requires clear nomenclature to ensure that all variables are tracked and not misused. Then, the extended Kalman filter used will be developed.

3.1   The "Rosetta Stone"

To keep track of the navigation states for each of the individuals or vehicles the following navigation state descriptor was created for each vehicle. First the Pinson states were addressed by assigning an index of each vehicle's position, velocity and attitude. Then if additional states are needed, such as accelerometer bias, they are also included into the vehicle's descriptor. Once all the additional states are added, the landmark states are added and the descriptors are included. These descriptors are used throughout the code to identified the state locations in a succinct manner. This means that at any point in the code, it is easy to determine the state index for any particular error type, vehicle or landmark.

3.2   State Model

In this section, the individual soldier's states and noises are defined. For clarification, vehicles are synonymous with soldiers. First, the individual variable will be defined. $\delta \mathbf{P}$ is the initial position error vector with components δx, δy, and δz representing the errors in the n-frame (NED) respectively. W_P represents the dynamic driving noise with NED components w_x, w_y, and w_z. The following states are for each individual vehicle.

$$\delta \mathbf{P} = \begin{bmatrix} \delta x & \delta y & \delta z \end{bmatrix}^T \qquad W_{\mathbf{P}} = \begin{bmatrix} w_x & w_y & w_z \end{bmatrix}^T$$

Next $\delta \mathbf{V}$ is the initial velocity error vector with components $\delta \dot{x}$, $\delta \dot{y}$, and $\delta \dot{z}$ representing the errors in the NED respectively. W_V represents the dynamic driving noise of the velocity and w_x, w_y, and wz.

$$\delta \mathbf{V} = \begin{bmatrix} \delta \dot{x} & \delta \dot{y} & \delta \dot{z} \end{bmatrix}^T \qquad W_V = \begin{bmatrix} w_{\dot{x}} & w_{\dot{y}} & w_{\dot{z}} \end{bmatrix}^T$$

$\delta \varepsilon$ is the initial attitude error vector with components $\delta \varepsilon_x$, $\delta \varepsilon_y$, and $\delta \varepsilon_z$ representing the errors in the NED respectively. W_ε represents the dynamic driving noise of the attitude and $w_{\varepsilon x}$, $w_{\varepsilon y}$, and $w_{\varepsilon z}$.

$$\delta \boldsymbol{\varepsilon} = \begin{bmatrix} \delta \varepsilon_x & \delta \varepsilon_y & \delta \varepsilon_z \end{bmatrix}^T \qquad W_\varepsilon = \begin{bmatrix} w_{\varepsilon x} & w_{\varepsilon y} & w_{\varepsilon z} \end{bmatrix}^T$$

With the first nine Pinson states and driving noises defined, the gyroscope and accelerometer bias error states and driving noises will now be defined. First the gyroscope error vector $\delta \mathbf{g}$ is made up of components δg_x, δg_y, and δg_z representing the gyroscope errors in the body frame respectively. W_g represents the dynamic driving noise with body frame components w_{g_x}, w_{g_y}, and w_{g_z}.

$$\delta \mathbf{g} = \begin{bmatrix} \delta g_x & \delta g_y & \delta g_z \end{bmatrix}^T \qquad W_{\mathbf{g}} = \begin{bmatrix} w_{g_x} & w_{g_y} & w_{g_z} \end{bmatrix}^T$$

Next the accelerometers error vector $\delta \mathbf{a}$ is made up of components δ_{a_x}, δ_{a_y}, and δ_{a_z} representing acceleration errors in the body frame. W_a represents the dynamic driving noise with body frame components w_{a_x}, w_{a_y}, and w_{a_z}.

$$\delta \mathbf{a} = \begin{bmatrix} \delta a_x & \delta a_y & \delta a_z \end{bmatrix}^T \qquad W_{\mathbf{a}} = \begin{bmatrix} w_{a_x} & w_{a_y} & w_{a_z} \end{bmatrix}^T$$

Next, the position states for the image landmarks will be denoted as $\mathbf{T}_n$ with NED components T_x, T_y, and T_z. The targets are modeled as stationary with random walk to prevent the filter from converging [5] and [8]. $W_{\mathbf{T}_N}$ represents the dynamic driving noise.

$$\mathbf{T}_n = \begin{bmatrix} T_x & T_z & T_z \end{bmatrix}^T \qquad W_{\mathbf{T}_N} = \begin{bmatrix} w_{T_x} & w_{Ty} & w_{T_z} \end{bmatrix}^T$$

The states are then combined for each vehicle into the standard Pinson states, accelerometer, and gyroscope. For vehicle m, this would be represented as

$$\mathbf{X}_m = \begin{bmatrix} \delta\mathbf{P} & \delta\mathbf{V} & \delta\boldsymbol{\varepsilon} & \delta\mathbf{g} & \delta\mathbf{a} & \mathbf{T}_{1_m} \cdots T_{n_m} {}_m \end{bmatrix}^T \tag{3.1}$$

Note that there are a total of n possible targets.

The states are further combined as $\mathbf{X}_M$ for each vehicle and $\mathbf{T}_N$ for the target for each vehicles.

The total state vector is then formed by combining state vectors from each vehicle (using a total of M vehicles).

$$\mathbf{X}_M = \begin{bmatrix} \mathbf{X}_1 & \mathbf{X}_2 & \cdots & \mathbf{X}_m \end{bmatrix}^T \tag{3.2}$$

The matrix used to describe the state dynamics or the $\mathbf{F}$ matrix is the next step in the filter design. This description will be for individual vehicle. The detailed description of the error dynamics are covered in Chapter 2. This will be divided up into sections so that it can more easily be described. First are the Pinson states. The full Pinson model is show in Equation (3.3) from [8]. This also includes the dynamics for the gyroscope and then the accelerometer states.

$$\mathbf{F}_{11_m} = \begin{bmatrix} 0_3 & \mathbf{I}_3 & 0_3 & 0_3 & 0_3 \\ \mathbf{C}_e^n\mathbf{G}\mathbf{C}_n^e & -2\mathbf{C}_e^n\mathbf{\Omega}_{ie}^e\mathbf{C}_n^e & (\mathbf{f}^n\times) & \mathbf{C}_b^n & 0_3 \\ 0_3 & 0_3 & -(\mathbf{C}_e^n\boldsymbol{\omega}_{ie}^e) & 0_3 & -\mathbf{C}_b^n \\ 0_3 & 0_3 & 0_3 & -\frac{1}{\tau_a}\mathbf{I}_3 & 0_3 \\ 0_3 & 0_3 & 0_3 & 0_3 & \frac{1}{\tau_b}\mathbf{I}_3 \end{bmatrix} \qquad (3.3)$$

Since the landmarks are modeled as stationary, there are no dynamics, and the dynamics matrix is the zero matrix.

$$\mathbf{F}_{22_m} = \left[0_{3_N \times 3_N}\right] \qquad (3.4)$$

Where N is the number of landmarks max.

With the individual vehicle state's identified, they are then combined for the full $\mathbf{F}$ matrix for each vehicle as

$$\mathbf{F}_m = \begin{bmatrix} \mathbf{F}_{11_m} & 0 \\ 0 & \mathbf{F}_{22_m} \end{bmatrix} \qquad (3.5)$$

Where m is the number representing the vehicle.

Finally the full $\mathbf{F}$ is defined as

$$\mathbf{F} = \begin{bmatrix} \mathbf{F}_1 & 0 & 0 & 0 \\ 0 & \mathbf{F}_2 & 0 & 0 \\ 0 & 0 & \ddots & 0 \\ 0 & 0 & 0 & \mathbf{F}_M \end{bmatrix} \qquad (3.6)$$

Where M is the total number of vehicles.

3.3 Measurement Model

The measurement matrix for the various types of measurements (radio, GPS, and, barometer) can now be defined. $\mathbf{H}$ is the collection of the different measurements that are currently available. $\mathbf{H}_{radio_{jk}}$ represent the measurements for the inter-vehicle radio ranging. $\mathbf{H}_{fived\_radio_1}$ is the influence matrix for the vehicle to fixed radio position. $\mathbf{H}_{baro_1}$ is the influence matrix for the barometric measurements. The last influence matrix is $\mathbf{H}_{landmark_1}$ for the images landmark measurements.

$$\mathbf{H}_{radio} = \begin{bmatrix} H_{radio_{jk}} & \cdots & H_{radio_R} \end{bmatrix}^T \tag{3.7}$$

$$\mathbf{H}_{fived\_radio} = \begin{bmatrix} H_{fived\_radio_1} & \cdots & H_{fived\_radio_L} \end{bmatrix}^T \tag{3.8}$$

$$\mathbf{H}_{baro} = \begin{bmatrix} H_{baro_1} & \cdots & H_{baro_M} \end{bmatrix}^T \tag{3.9}$$

$$\mathbf{H}_{landmark} = \begin{bmatrix} H_{landmark_1} & \cdots & H_{landmark_N} \end{bmatrix}^T \tag{3.10}$$

$$\mathbf{H} = \begin{bmatrix} \mathbf{H}_{radio} & \mathbf{H}_{fived\_radio} & \mathbf{H}_{baro} & \mathbf{H}_{landmark} \end{bmatrix}^T \tag{3.11a}$$

To develop the Kalman filer to investigate the performance of the ranging radios, the measurement model for each of the sensors is required. The measurement model for the ranging radio between vehicles i and j is the following

$$X = x_{INS_i} + \delta x_i - x_{INS_j} - \delta x_j \tag{3.12}$$

$$Y = y_{INS_i} + \delta y_i - y_{INS_j} - \delta y_j \tag{3.13}$$

$$Z = z_{INS_i} + \delta z_i - z_{INS_j} - \delta z_j \tag{3.14}$$

$$h_{radio_{ij}} = \sqrt{X^2 + Y^2 + Z^2} \tag{3.15}$$

The measurement noises are independent, zero-mean, Gaussian noises with

$$E[v_r v_r] = \boldsymbol{\sigma}_r^2 \tag{3.16}$$

$$Z_{radio_{jk}} = h_{radio_{jk}} + v_r \tag{3.17}$$

The perturbation technique is used to linearize $\mathbf{h}_{radio_{jk}}$ about the nominal state resulting in

$$H_{radio_{jk}} = \frac{\partial h_{radio_{jk}}(\mathbf{x})}{\partial \mathbf{x}} \bigg|_{\mathbf{x}=\hat{\mathbf{x}}} \tag{3.18}$$

The fixed radio is almost identical to the inter vehicle ranging case the difference being is that the fixed radio is at a known location. This changes h to

$$h_{fixed\_radio_{jl}} = \sqrt{(x_{INS_i} + \delta x_i - x_l)^2 + (y_{INS_i} + \delta y_i - y_l)^2 + (z_{INS_i} + \delta z_i - z_l)^2} \tag{3.19}$$

Where the position of the fixed radio l is given as $[x_l \ y_l \ z_l]^T$.

The measurement noise is independent, zero-mean, Gaussian noises with

$$E[v_r v_r] = \sigma_r^2 \tag{3.20}$$

$$Z_{fixed\_radio_{jl}} = h_{fixed\_radio_{jl}} + v_r \qquad (3.21)$$

The perturbation technique is used to linearize $\mathbf{h}_{fixed\_radio_{jl}}$ about the nominal state resulting in

$$H_{fixed\_radio_{jl}} = \frac{\partial h_{fixed\_radio_{jl}}(\mathbf{x})}{\partial \mathbf{x}} \big|_{\mathbf{x}-\hat{\mathbf{x}}} \qquad (3.22)$$

Now the barometric aid measurement will be found. The barometric altimeter is modeled as

$$Z_{baro_m} = z_{ins_m} + \delta z_{ins_m} + v_b \qquad (3.23)$$

The statistics for the barometric measurement noise are

$$E[v_b v] = \sigma^2 \delta_{ij} \qquad (3.24)$$

The image measurements will now be defined by closely following the work presented in [8]. A monocular camera configuration is best for dismounted soldiers, because size and weight are critical to combat operations. First, the landmark's initial location estimate y^n is found for a feature of interest z given the direction associated with the pixel location and the distance which is measured, using a coded aperture.

The vector from the camera to the target is defined as

$$\underline{s}^c = \mathbf{T}^c_{pic}\underline{z} \qquad (3.25)$$

The landmark location is found by

$$\mathbf{y}^n = \mathbf{p}^n + \mathbf{C}_b^n \left[\mathbf{p}_{cam}^b + \mathbf{dC}_c^n \underline{\mathbf{s}}^c \right] \tag{3.26}$$

Where d represents the distance to the landmark and is found from the z component of $\mathbf{y}^n$, $\mathbf{p}_{cam}^b$, and $\underline{\mathbf{s}}^c$.

$$\mathbf{d} = \frac{[\mathbf{y}^n]_z - \left[\mathbf{p}^n + \mathbf{C}_b^n \mathbf{p}_{cam}^b \right]_z}{\left[\mathbf{C}_b^n \mathbf{C}_c^b \underline{\mathbf{s}}^c \right]_z} \tag{3.27}$$

Now the position of the landmark is found and the influence matrix for the uncertainty can be found for the pixel.

$$\mathbf{H}_{zy_j} = \frac{\partial \mathbf{z}}{\partial \mathbf{y}^n} \tag{3.28}$$

$$\mathbf{H}_{zy} = \mathbf{T}_c^{pix} \frac{\mathbf{s}_z^c \frac{\partial \mathbf{s}^c}{\partial \mathbf{y}^n} - \mathbf{s}^c \left[\frac{\partial \mathbf{s}^c}{\partial \mathbf{y}^n} \right]_z}{\left(\mathbf{s}_z^c \right)^2} \tag{3.29}$$

and

$$\frac{\partial \mathbf{s}^c}{\partial \mathbf{y}^n} = \mathbf{C}_b^c \mathbf{C}_n^b \tag{3.30}$$

$\mathbf{H}_{zy_j}$ represents the partial derivatives with respect to the pixel coordinates. In addition with range measurements, there is another row in the $\mathbf{H}$ matrix that is equivalent in form to the fixed radio $\mathbf{H}$ matrix in Figure 2.2.

3.4 Generated Test Data

To test whether imaging would assist the radio positioning, the following test case was developed. The scenario is for Stryker Brigades. The terrain is a moderately sloping canyon with low level vegetation, and the forestation has a medium canopy. There is a road running parallel to the bottom of the canyon. There are three groups each of which has two dismounted soldiers. The first group would move down the
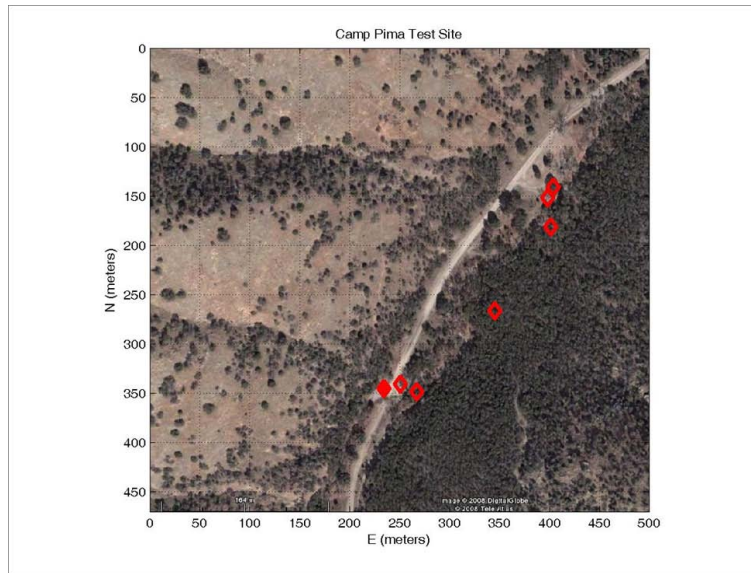
Figure 3.1: This figure shows a picture of the terrain in senario used in the simulation

center of the canyon and the other two groups would flank the first on the right and the left. The Stryker vehicles would be positioned around the soldiers. The first two Strykers would be forward of the soldiers and at the end of the soldier's trajectory. The second two Strykers would start on the road in close proximity to where the soldiers trajectory starts.

To simulate this scenario, the troops are modeled as having a random walk that is constrained in heading to follow a straight line trajectory down the valley. The Strykers are modeled as fixed radios with the moving vehicles positioned at a point northwest of the trajectories. This would generate the same geometry that would be observed if the moving vehicles were moving along the road with the soldiers. Figures 3.1 shows lightly sloping valley the terrain that the scenario is based on. Figure ?? shows the actual paths that the troops are following along the bottom of the valley. It can be see that the soldiers are starting at about -100 meters on the north axis and 400 meters on the east axis all in the NED frame. The fixed radios are located as seen, with heights of (20m, 25m, 20m) from left to right in Figure ??.
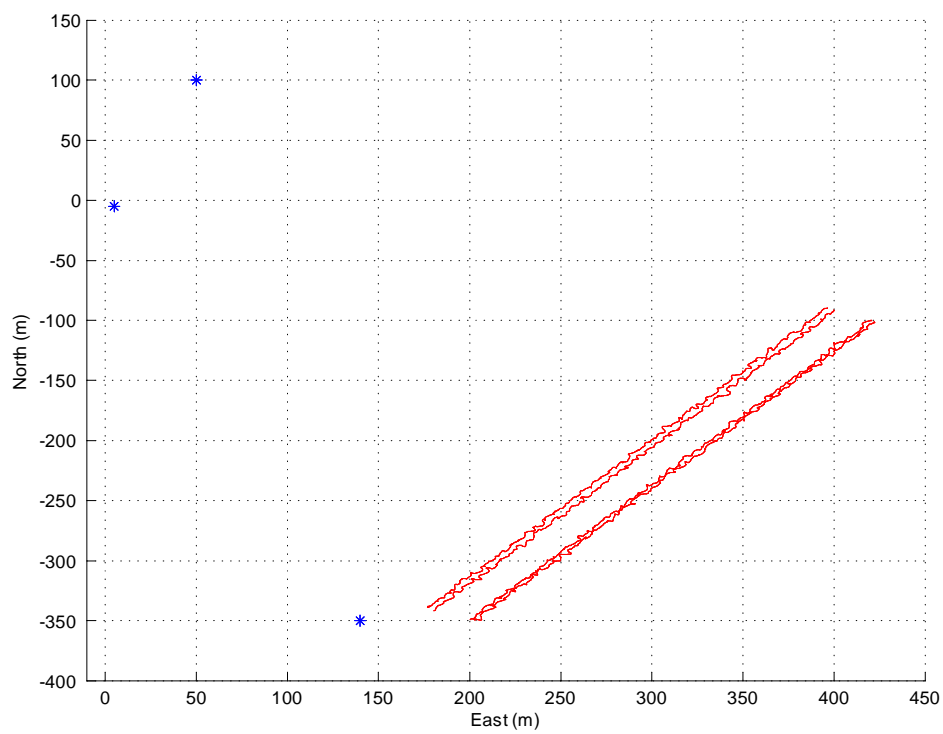
Figure 3.2: This figure shows the actual trajectories of the the four soldiers (Red) and the locations of the fixed radios (Blue)
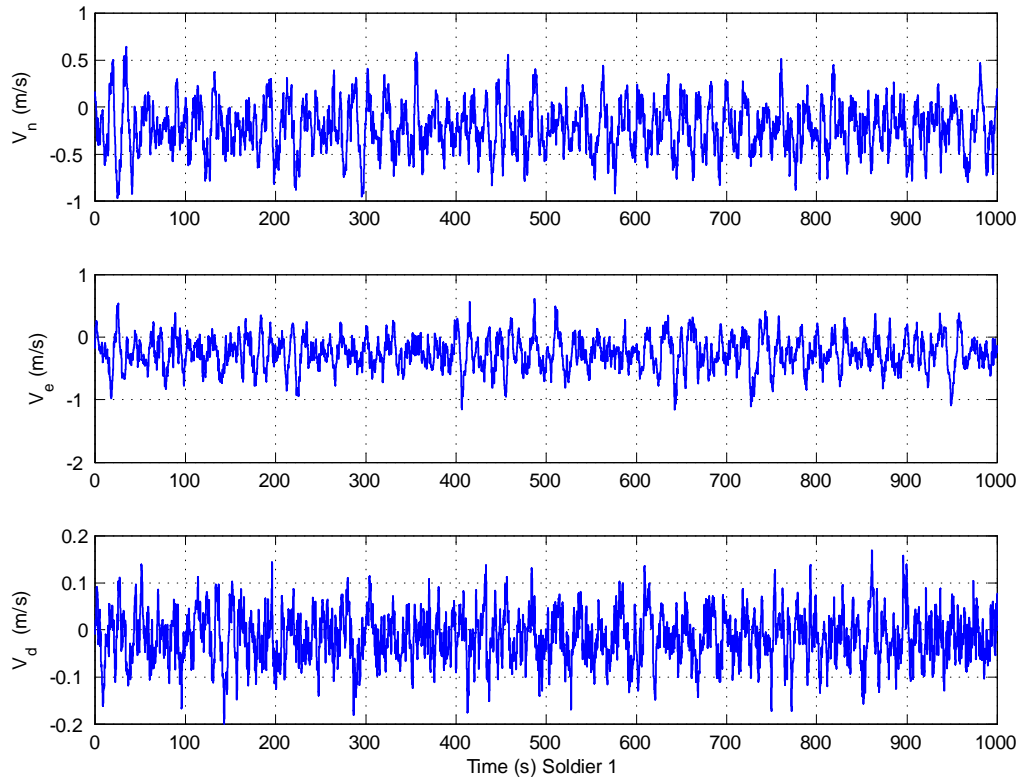
Figure 3.3: This figure is the acutal velocity of Soldier-1 for run 1 in scenario 1

Figure 3.3 and 3.4 are the true velocity and attitude of a soldier moving through the scenario.

Note the heading in Figure 3.4 is fluctuating about $\pm 57°$.

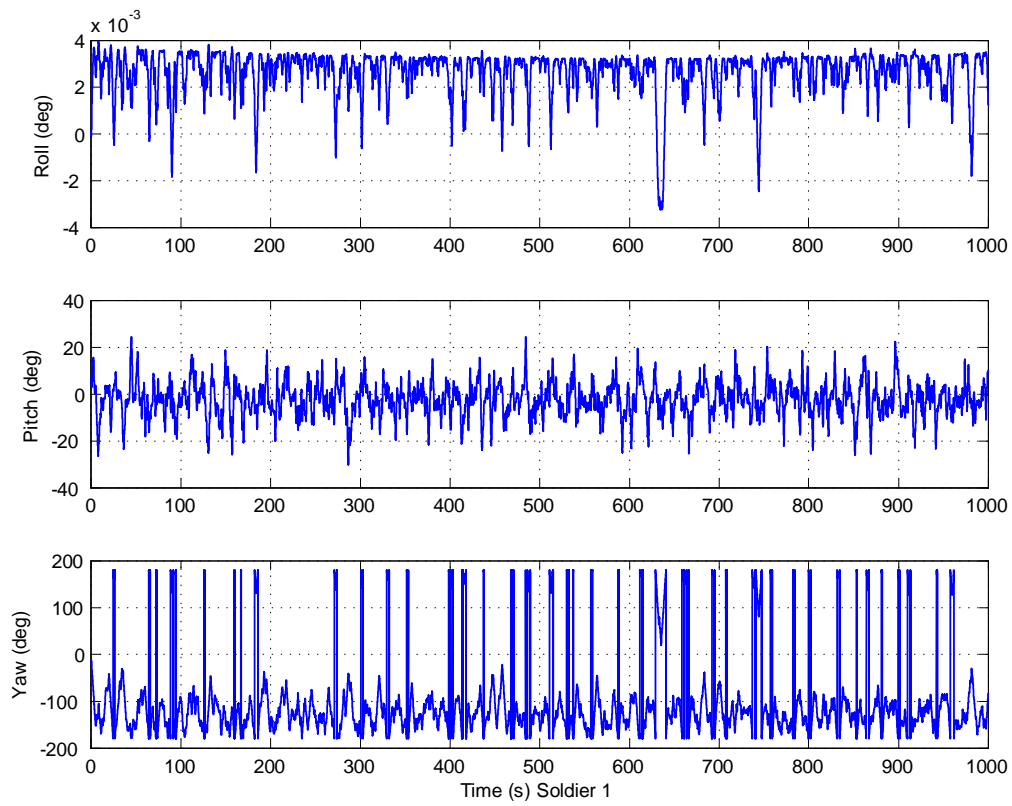Figure 3.4: This figure is the Acutal Attitude of Soldier-1 for run 1 in Scenario 1

IV. Simulation and Results

To test that the vision measurements will improve the radio positioning, the filter developed in Chapter 3 was implemented in software. The software simulation was written in MATLAB and is based upon software originally developed in [8]. The filters were run on the scenario developed in Chapter 3. This scenario was tested in two cases–one with inter-vehicle radio, fixed radio, and barometric measurements; and, one with all the measurements from the first case plus image measurements. The simulation was run three times each for cases with two and four soldiers. A six soldiers case was tried and it was found that, after approximately 100 seconds, numerical precision issues began to arise. Due to time constraints these issues were not investigated further. Apart from the numerical precision issues, the six vehicle case required 17.5 hours in MATLAB 2008b on a 6600 quad core running approximately at 90% on all processors.

For each of the scenarios, plots of the north, east, and down position errors were generated with a filter computed 2 sigma error. A table was also created with all the root mean square (RMS) values for each vehicle across time and across all vehicles and all time. Root mean square horizontal (RMS-H) values are also generated for each vehicle across time and across all vehicles and all time.

During testing it was found that if the images were incorporated after the radio measurements, the image features became almost impossible to track, and only one or two features could be tracked between epochs. With the images incorporated before the measurements, feature tracking was much more effective. It is believed that this is due to the large variation in position due to the high radio standard deviation. In theory, the order in which measurements are incorporated into the filter should not make any difference. However, since this is an extended Kalman filter, relinearization occurs after each measurement is incorporated, so it is best to incorporate the "strongest" measurements first.

Table 4.1: Test Scenario 1 2: Radio Only case, Two Soldiers case, NED frame

Parameters	1-σ (Units)
Radio Ranging (std.)	20 m
Barometer (std.)	10 m

Throughout chapter 4 the term 'radio only' is used when all tests incorporate barometric measurements. This nomenclature is used with the understanding that barometric measurements are always used.

4.1 Test Scenario 1: Radio only, 2 Soldiers

The first test consisted of two soldiers with inter-vehicle ranging radios and three fixed radio measurements. Two were stationary at a far distance representing the moving Strykers and one fixed at the end of the soldiers' trajectory. Table 4.1 contains the test parameters used in the EKF.

As seen in Figure 4.1, the filter performance for Soldier 1 appears to be consistent with 2-σ bounds for north, east, and down positions.

In Figure 4.2 for Soldier 1, the north, east, and down plots were consistent with 2-σ level. There seams to be no issues regarding the velocity estimates.

In Figure 4.3 for Soldier 1, the north and east track are consistent with 2-σ level. This is not the case for the down axis. These start off well and then become almost oscillatory. This will show up in all the attitude plots about the down axis for the radio only cases. This is an indication that heading could pose an issue that will need to be addressed. The trajectory that the soldiers follow has considerable heading changes that could also be adding to this issue. This large heading change phenomena was apparent during the generation feature as they plotted.

The plots of positions, velocity, and attitude for the other soldiers are very similar and require no further comment. All the test scenarios (1,2, 3 and 4) plots can however be found the Appendix.
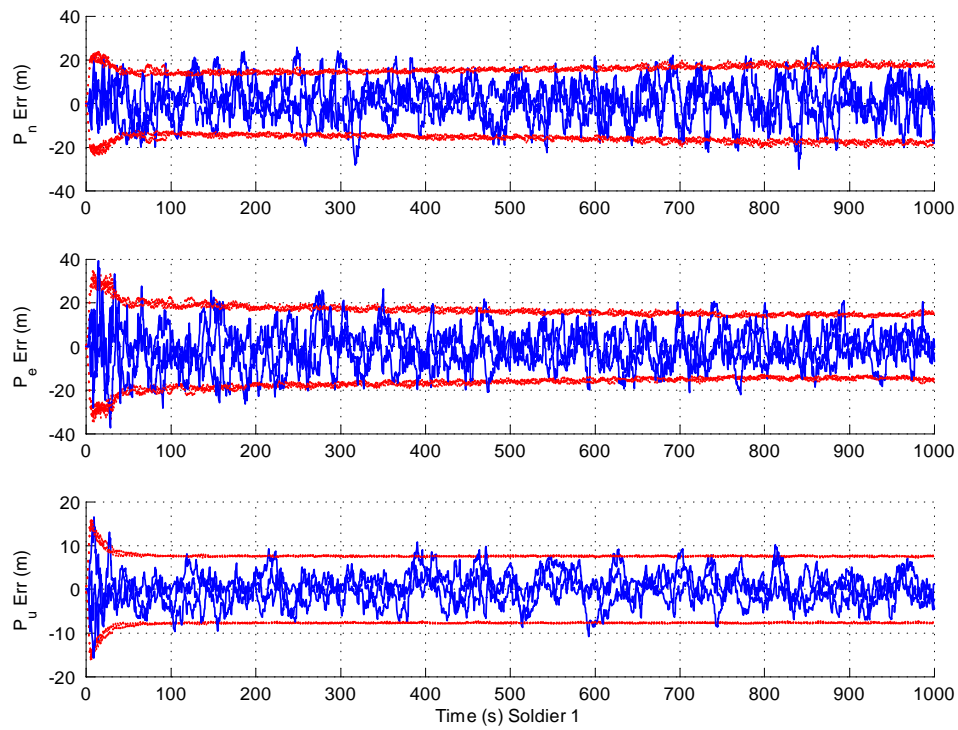
Figure 4.1: Test Scenario 1: Radio Only-2 Soldiers case, Soldier 1, Position Error in NED (Blue), Filter Calculated Error 2-σ (Red), 3 Monte-Carlo Runs
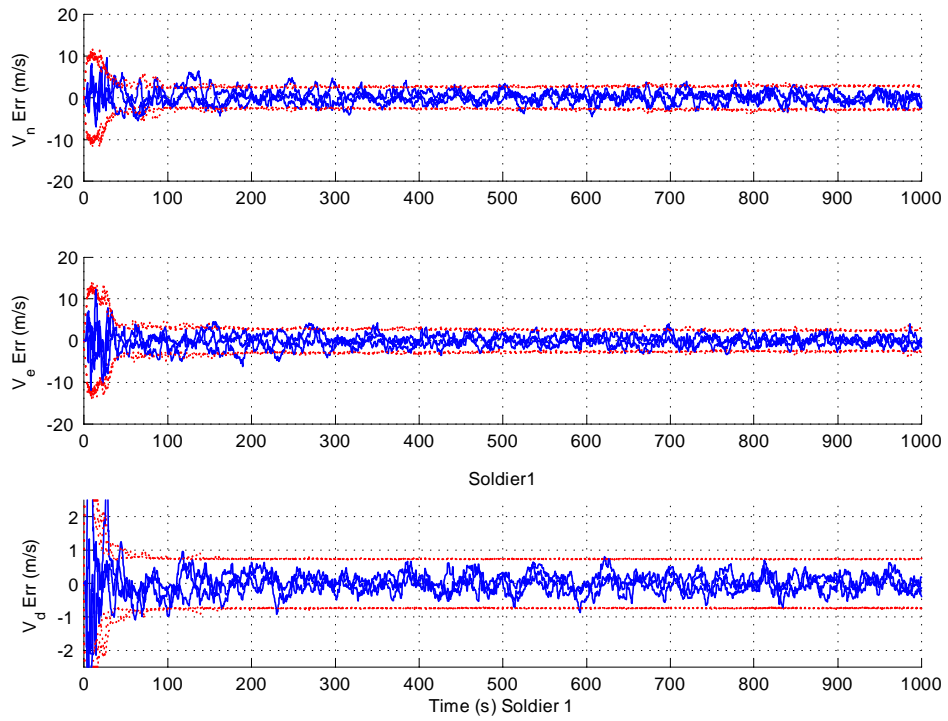
Figure 4.2: Test Scenario 1: Radio Only-2 Soldiers case, Soldier 1, Velocity Error in NED (Blue), Filter Calculated Error 2-σ (Red), 3 Monte-Carlo Runs
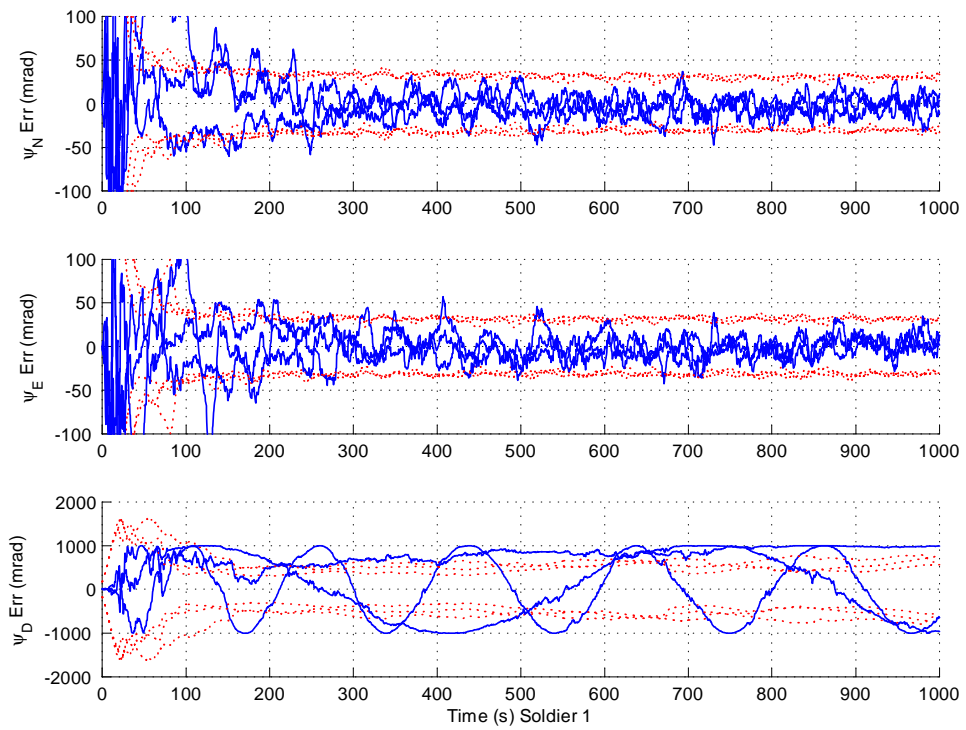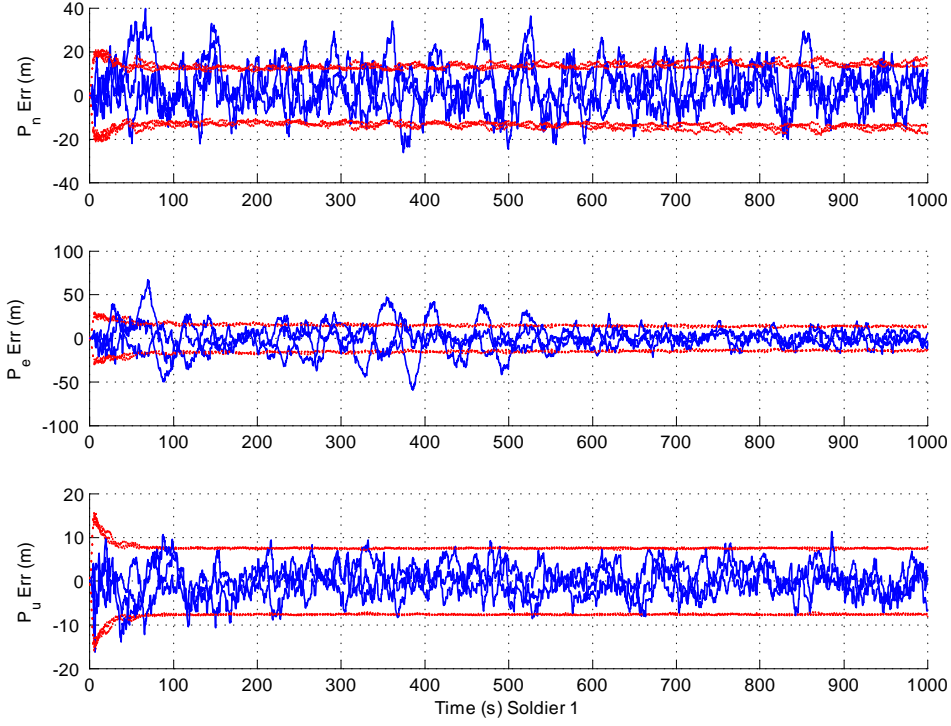
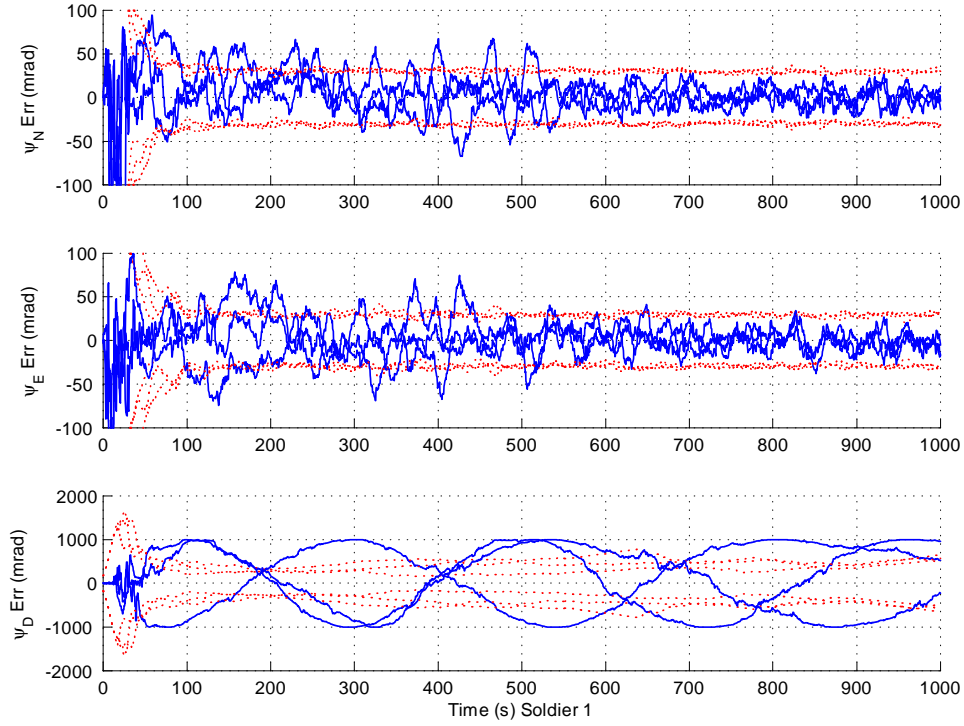Figure 4.3: Test Scenario 1: Radio Only-2 Soldiers case, Soldier 1, Attitude Error in NED (Blue), Filter Calculated Error 2-σ (Red), 3 Monte-Carlo Runs

Table 4.2: Test Scenario 1: Radio Only case, Two Soldiers case, NED frame

	RMS-N (m)	RMS-E (m)	RMS-D (m)	RMS-H (m)
Run 1 Soldier 1	8.19	8.19	3.11	11.58
Run 1 Soldier 2	9.70	9.89	3.67	13.86
Run 2 Soldier 1	7.88	9.03	3.53	11.99
Run 2 Soldier 2	9.22	11.73	3.95	14.92
Run 3 Soldier 1	8.85	8.18	3.33	12.05
Run 3 Soldier 2	9.91	9.23	4.07	13.54
All Runs All Soldiers	8.96	9.37	3.61	12.99

As can be seen in Table 4.2 the results for the soldiers are generally consistent between soldiers.

4.2   Test Scenario 2: Radio only, 4 Soldiers

The second test is for the four soldier scenario with the same configurations as the first test scenario.

Figure 4.4 results are similar to Scenario 1 with slightly higher errors in the NED position. This can be seen comparing Figures 4.1 and Figure 4.4.

The attitude errors are almost identical to the two soldier case comparing Figure 4.2 and Figure 4.5.

It appears that adding more vehicles to the solution adds a small amount of uncertainty to the solution. This is evident in Table 4.3. The results remain similar between the soldiers which is constant with Figures 4.1 through 4.5.

4.3   Test Scenario 3: Radio and Images, 2 Soldier

The third test consisted again of two soldiers with inter-vehicle ranging radio and three fixed radio measurements, but now the image measurements were incorporated. As seen in Table 4.4 filter parameters are similar to scenario 1 with the imaging added for the pixels and the monocular slant range.
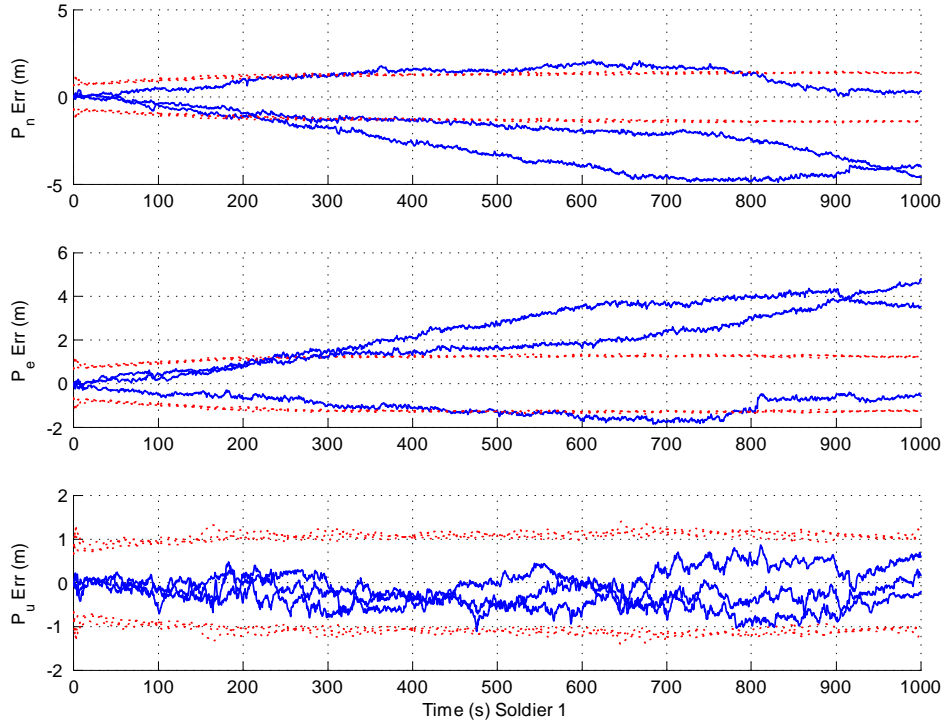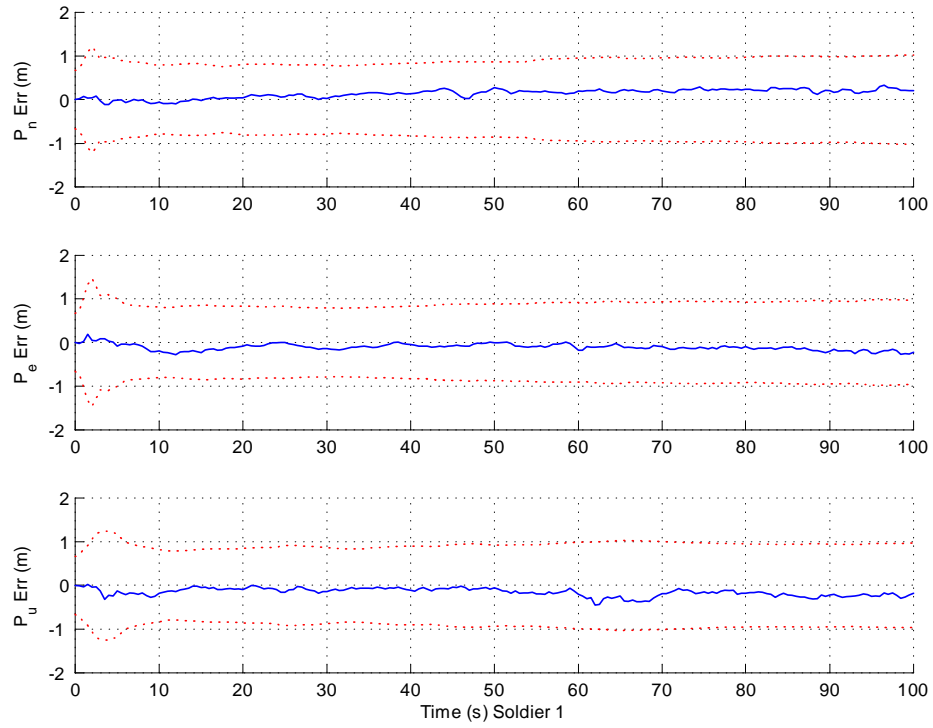
Figure 4.4: Test Scenario 2: Radio Only-4 Soldiers case, Soldier 1, Position Error in NED (Blue), Filter Calculated Error 2-σ (Red), 3 Monte-Carlo Runs

Table 4.3: Test Scenario 2: Radio Only case, Four Soldiers case, NED frame

|	RMS-N (m)	RMS-E (m)	RMS-D (m)	RMS-H (m)
Run 1 Soldier 1	10.93	16.64	3.42	19.91
Run 1 Soldier 2	11.08	16.85	3.94	20.17
Run 1 Soldier 3	14.84	23.80	3.73	28.04
Run 1 Soldier 4	16.47	29.81	4.04	34.06
Run 2 Soldier 1	9.04	9.70	3.34	13.26
Run 2 Soldier 2	10.48	12.40	3.53	16.45
Run 2 Soldier 3	12.87	20.39	4.56	24.11
Run 2 Soldier 4	11.99	13.99	3.59	18.42
Run 3 Soldier 1	9.78	11.98	3.44	15.46
Run 3 Soldier 2	9.97	14.50	3.76	17.59
Run 3 Soldier 3	16.71	23.81	4.57	29.09
Run 3 Soldier 4	9.85	15.47	3.88	18.34
All Runs All Soldiers	12.00	17.45	3.82	21.24

Figure 4.5: Test Scenario 2: Radio Only-4 Soldiers case, Soldier 1, Attitude Error in NED (Blue), Filter Calculated Error 2-σ (Red), 3 Monte-Carlo Runs

Table 4.4: Test Scenarios 3 4: Radio and Image case, NED frame

Parameters	1-σ (Units)
Radio Ranging (std.)	20 (m)
Barometer (std.)	10 (m)
Image (std.)	1 (pixel)
Image slant range (std.)	5 (m)

Figure 4.6: Test Scenario 3: Radio and Image-2 Soldiers case, Soldier 1, Position Error in NED (Blue), Filter Calculated Error 2-σ (Red), 3 Monte-Carlo Runs

As seen in Figure 4.6 there is immediately a difference in scale. The errors are reduced significantly from the radio only case (Figure 4.1). While the covariance is around 1 m the error grows up to around 5 m for north and east. This is better than the 20 m that was found in Figure 4.1, but not consistent with the covariance that is created by the filter. Further tuning of the initial covariance could help correct this. There was one area in the MATLAB code that didn't have a baseline to verify performance gains and that was the monocular slant range. By testing the code without the slant range it was found that there is a problem within the code for the slant range as seen in Figure 4.7 . Due to time constraints this will have to be explored by further research.

The image measurement definitely aided the attitude error. As seen by comparing the Radio Only case (Figure 4.3) with the Radio and Image case (Figure 4.8), the images improved the attitude errors by more than an order of magnitude. This

Figure 4.7: Test Scenario 3 Special: Radio and Image-2 Soldiers case, Soldier 1, Position Error in NED (Blue), Filter Calculated Error 2-σ (Red), 1 Run 100 seconds
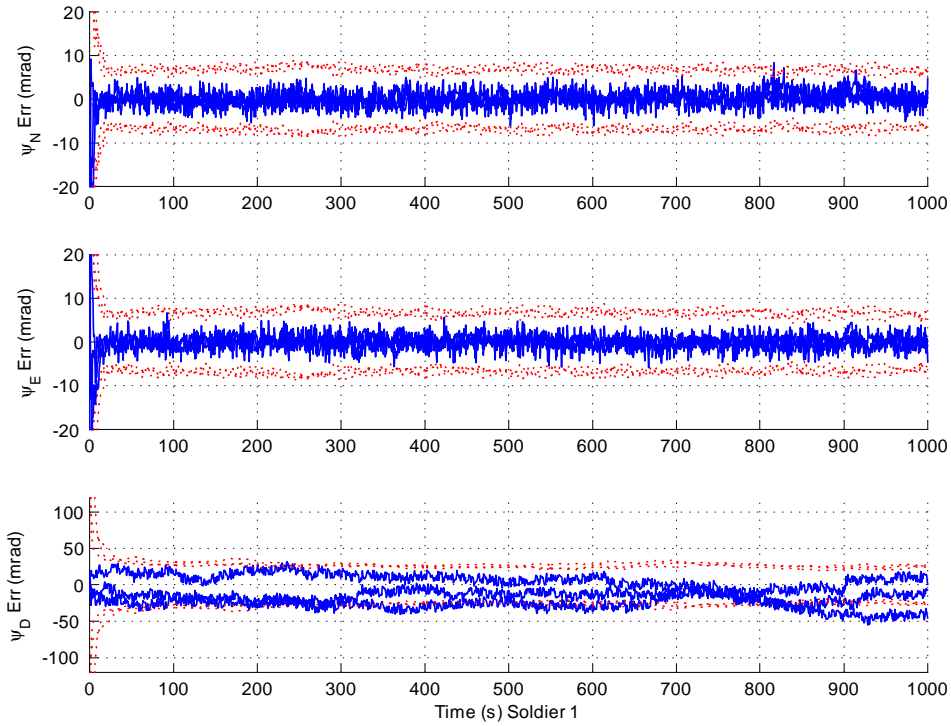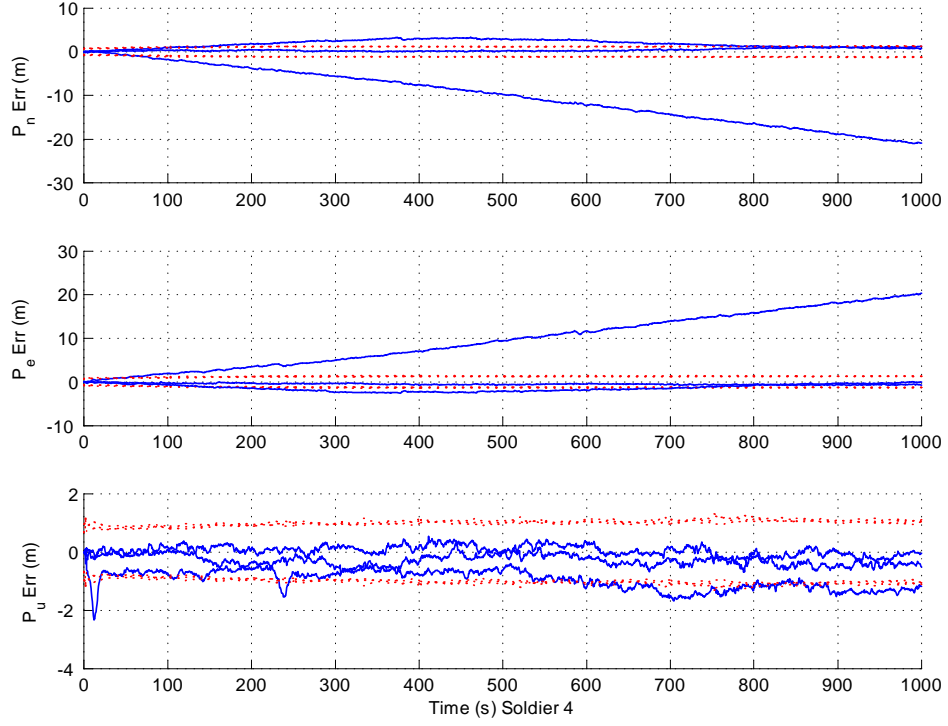
Figure 4.8: Test Scenario 3: Radio and Image-2 Soldiers case, Soldier 1, Attitude Error in NED (Blue), Filter Calculated Error 2-σ (Red), 3 Monte-Carlo Runs

finding adds to the importance of incorporating the image measurement before the radios.

The velocity plot is in the Appendix but doesn't show any beneficial information, however, the RMS values do. As seen in Table 4.5, Test Scenario 3 Radio only-2 Soldiers, the values are much smaller than those found in Test Scenario 3 Radio only-2 Soldiers of Table 4.2. It would appear that the slant range is truly effecting run 1's of Soldier one's. Comparing Table 4.5 and Table 4.2 there appears to be an improvement in the RMS error by a factor of approximately 2.

4.4 Test Scenario 4: Radio and Images, 4 Soldiers

The fourth test is again for the four soldier scenario with the same configurations as scenario 2 with image measurements incorporated. The results are shown in Figures 4.9-4.11.

Table 4.5: Test Scenario 3: Radio and Image case, Two Soldiers case, NED frame

	RMS-N (m)	RMS-E (m)	RMS-D (m)	RMS-H (m)
Run 1 Soldier 1	1.24	1.07	0.31	1.64
Run 1 Soldier 2	2.81	2.68	0.20	3.88
Run 2 Soldier 1	3.30	2.83	0.39	4.35
Run 2 Soldier 2	6.76	6.17	0.31	9.15
Run 3 Soldier 1	2.04	2.21	0.48	3.01
Run 3 Soldier 2	9.08	8.54	0.44	12.47
All Runs All Soldiers	4.21	3.92	0.36	5.75

For Figure 4.9 vehicle four has the drift problem as seen in scenario 3 for two vehicles with imaging and radio measurements. The slant range appears to be influencing it and overly improving the covariance.

Additional to the slant range effects in Figure 4.9 there are other effects from what appears to be heading errors allowing the solder to drift off as seen in Figure 4.10.

Figure 4.11 shows even better attitude correction, save one case that showed a biased error immediately. This again shows image adding improves the radio ranging in the case where the initial first 60 second of heading measurements are reasonably good.

The runs with heading errors starting at the beginning of the run have the highest RMS values. The data without large heading errors was slightly improved over scenario three. This can be seen by comparing Table 4.5 and Table 4.6. So, if image features are tracked reasonably well at the beginning of the run, the filter has a much better performance over the radio only cases. It is possible that further tuning of the filter would improve the ability of the filter to initially converge onto the correct attitude.

From reviewing the data, there are areas that need to be addressed in further research, like the image's slant range measurement and the heading errors. Over all, the system shows great promise for improving performance.
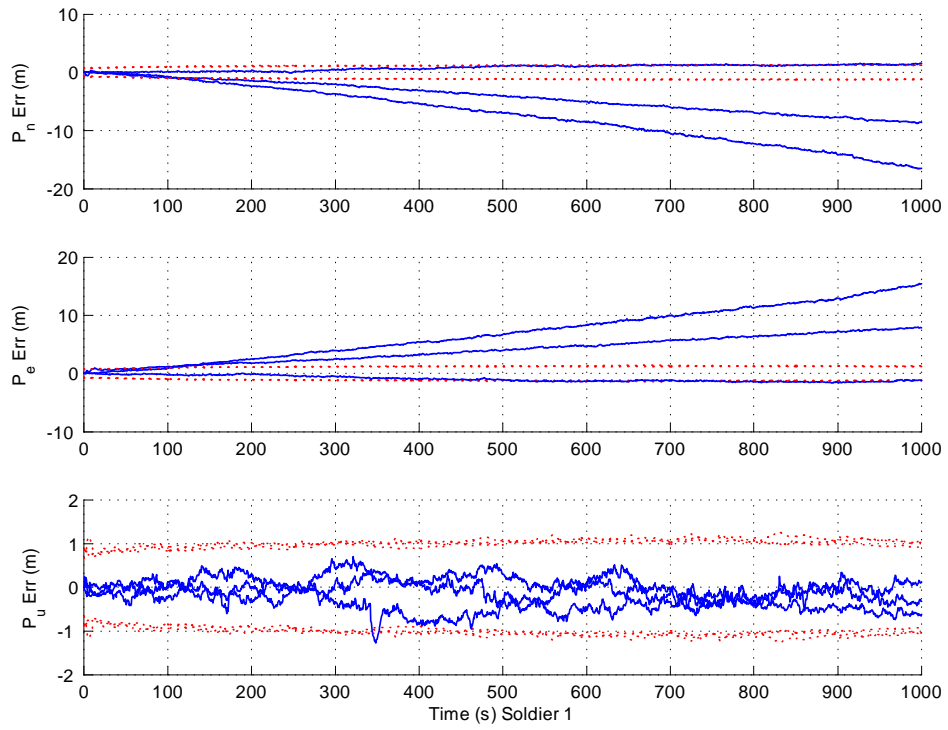
Figure 4.9: Test Scenario 4: Radio and Image-4 Soldiers case, Soldier 4, Position Error in NED (Blue), Filter Calculated Error 2-σ (Red), 3 Monte-Carlo Runs
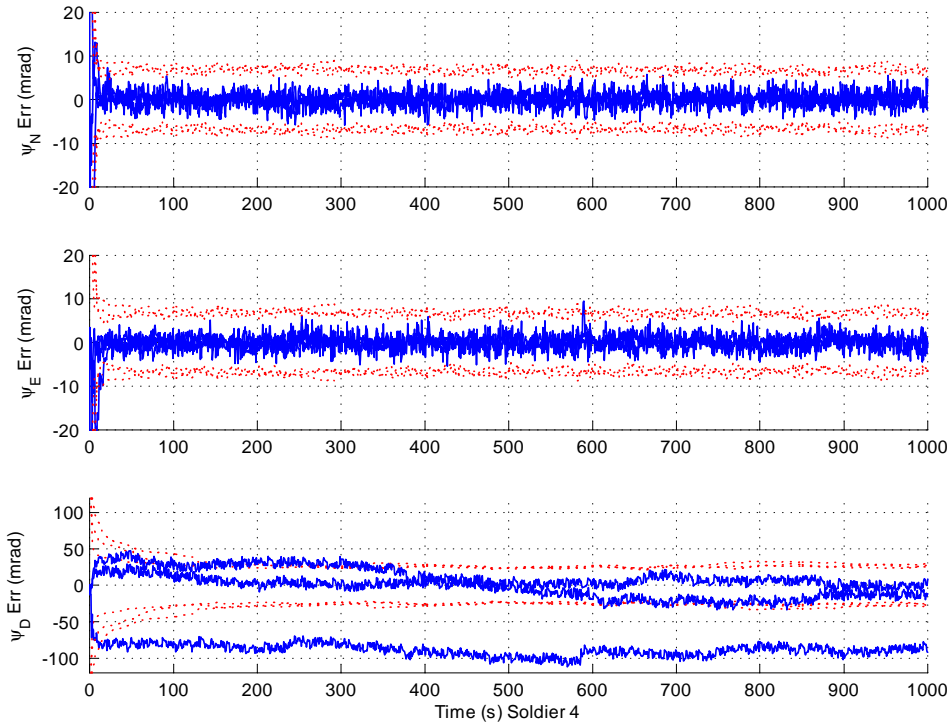
Table 4.6: Test Scenario 4: Radio and Image case, Four Soldiers case, NED frame

|	RMS-N (m)	RMS-E (m)	RMS-D (m)	RMS-H (m)
Run 1 Soldier 1	4.88	4.65	0.41	6.73
Run 2 Soldier 1	0.63	0.65	0.22	0.91
Run 3 Soldier 1	6.46	6.41	0.42	9.11
Run 1 Soldier 2	11.83	11.31	1.01	16.37
Run 2 Soldier 2	8.69	8.20	0.21	11.95
Run 3 Soldier 2	3.54	3.95	0.39	5.30
Run 1 Soldier 3	0.94	1.17	0.24	1.50
Run 2 Soldier 3	0.54	0.52	0.26	0.75
Run 3 Soldier 3	0.92	1.05	0.32	1.40
Run 1 Soldier 4	6.90	6.13	0.48	9.22
Run 2 Soldier 4	5.97	5.89	0.50	8.39
Run 3 Soldier 4	2.03	1.55	0.29	2.55
All Runs All Soldiers	4.44	4.29	0.40	6.18

Figure 4.10: Test Scenario 4: Radio and Image-4 Soldiers case, Soldier 1, Position Error in NED (Blue), Filter Calculated Error 2-σ (Red), 3 Monte-Carlo Runs

Figure 4.11: Test Scenario 4: Radio and Image-4 Soldiers case, Soldier 4, Attitude Error in NED (Blue), Filter Calculated Error 2-σ (Red), 3 Monte-Carlo Runs

# V. Conclusion and Recommendations

5.1 Conclusion

The results from the simulations were promising looking at Table 5.1. There is an improvement in the results and image measurements improve the capabilities of the radio ranging system. The improvement on all axis were on the order of approximately a factor of 2. There is good support that slant range measurements are causing issues, especially with respect to the slow drift of the error as seen in the position plots with imaging used. A test case with slant range only proved this as it didn't have a drift. An additional issue can also occur if the image measurements can't converge in the first minute of operation. Looking at larger Monte Carlo simulations of the simulation will help to verify how often the imaging can possibly have this error. Looking over Table 5.1 it was also discovered that as the number of soldiers increased there was an increase in the RMS error of a factor of approximately 1.3 for Scenarios 1 and 2. For Scenarios 3 and 4 there was an increase in RMS error again but it was only a factor of 1.08. It is possible that adding more vehicles acts like adding more process noise to the system as more vehicles are added but with imaging this is constrained

The centralized approach presented in this thesis forms a solid base for moving this research into distributed filter structures, such as [1].

As mentioned in Chapter 4, the order in which the measurements are incorporated is important to the filter. If a large noise measurement is incorporated into

Table 5.1: Test Senario 1-4 Both cases for All Soldiers

	RMS-N (m)	RMS-E (m)	RMS-D (m)	RMS-H (m)
Test Scenario 1: Radio Only-2 soldiers case, All Soldier	8.96	9.37	3.61	12.99
Test Scenario 2: Radio Only-4 soldiers case, All Soldier	12.00	17.45	3.82	21.24
Test Scenario3: Radio and Image-2 soldiers case, All Soldier	4.21	3.92	0.36	5.75
Test Scenario 4: Radio and Image-4 soldiers case, All Soldier	4.44	4.29	0.40	6.18

the position before the image measurement it can adversely effect the filters ability to track image features.

Bookkeeping techniques like the "Rosetta Stone" were crucial to tracking the many states that the filter had in its 4 and 6 soldier cases. Without such techniques the ability to delineate the different states of the soldiers and targets would have been more complicated and possibly less efficient at generating the covariance matrix $\mathbf{P}$ and the influence matrix $\mathbf{H}$.

5.2 Recommendations

With the initial simulations conducted, further tests should be made to see how the system will perform in other scenarios. As was already seen, numerical issues started to arise when six vehicles were simulated. There is also the possibility that the use of a partial filter could improve the estimates if there are any issues in linearization.

There are additional scenarios that could also be tested. Different conditions such as urban, large mountains and thicker foliage could be modeled. Scenarios from the troops in the field would be the best way to test real world scenarios. Once these have been simulated, field tests can be accomplished to determine a rigorous model of the radios to include issue like multipath and tropospheric delays. The work in single camera ranging should also be incorporated to make the monocular camera slant range measurement error model more precise.

The ability to match features between the different soldiers would be another step that could even further reduce the attitude errors that were seen by correlating the vehicle's heading.

The addition of other measurements could also continue to improve the estimate, like from one GPS satellite or some other signal.

VI. Appendix. Complete Collection Of Plots For Chapter Four
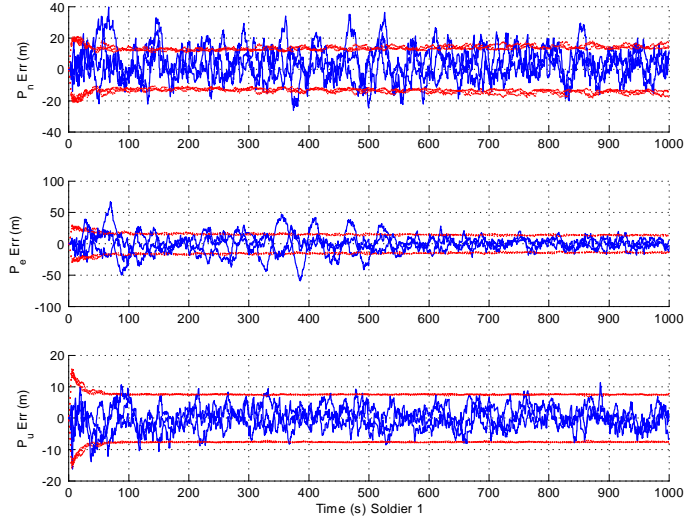
Test Scenario 2: Radio only, 2 Soldiers
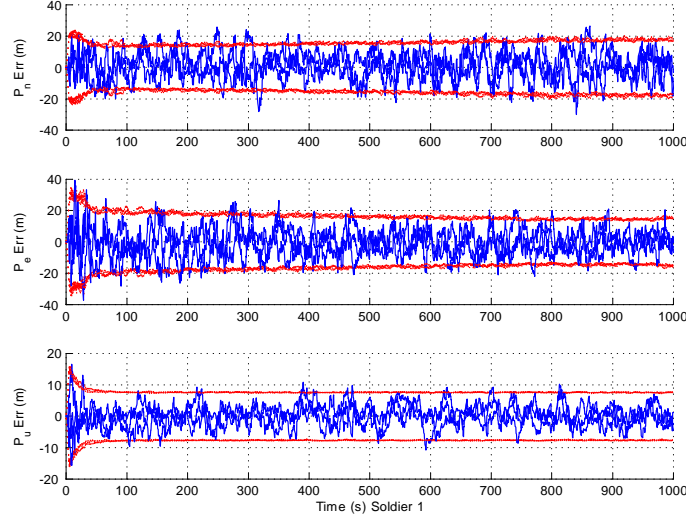
Figure 6.1: Test Scenario 1: Radio Only-2 Soldiers case, Soldier 1, Position Error in NED (Blue), Filter Calculated Error 2-σ (Red), 3 Monte-Carlo Runs
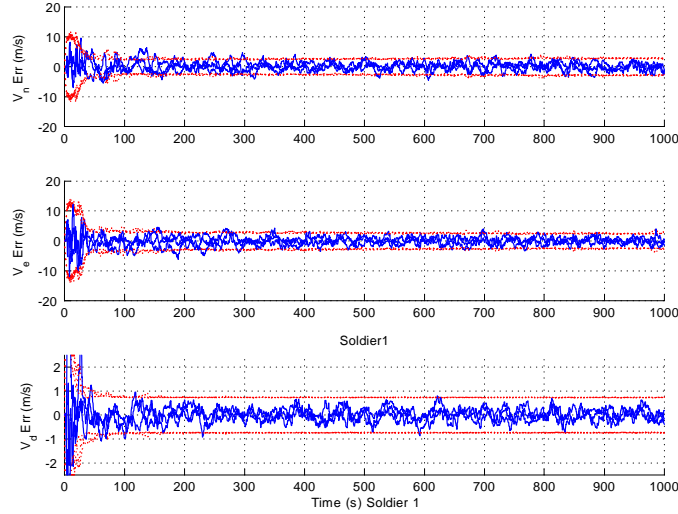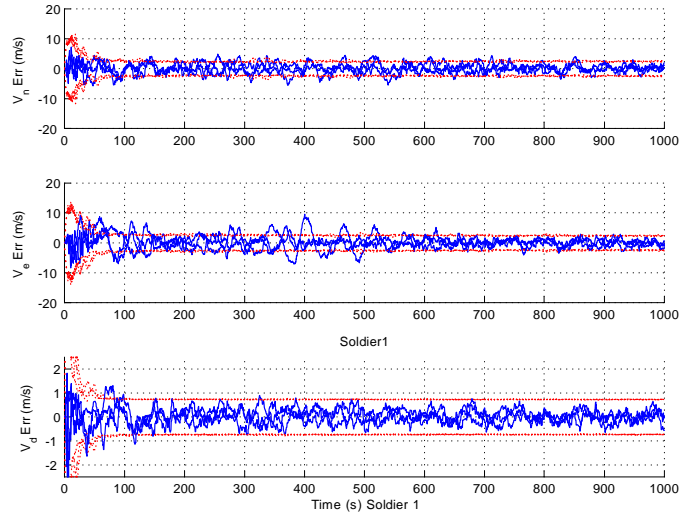

Figure 6.2: Test Scenario 1: Radio Only-2 Soldiers case, Soldier 1, Velocity Error in NED (Blue), Filter Calculated Error 2-σ (Red), 3 Monte-Carlo Runs
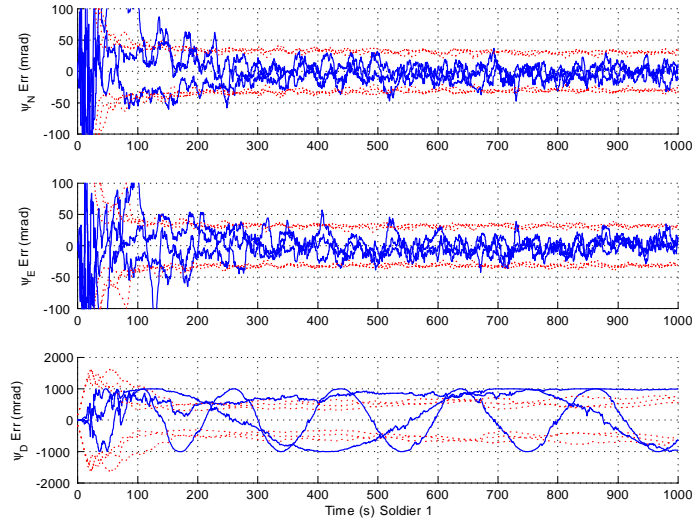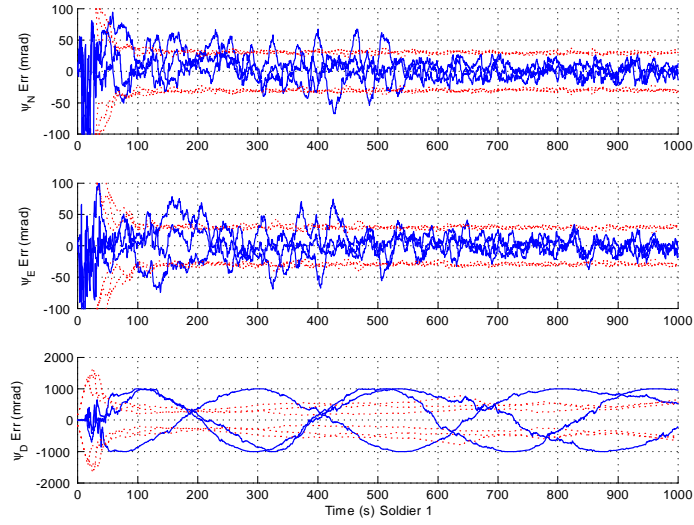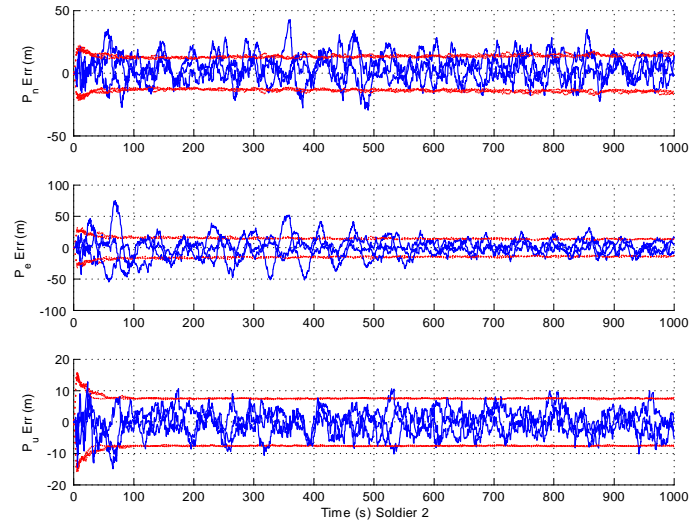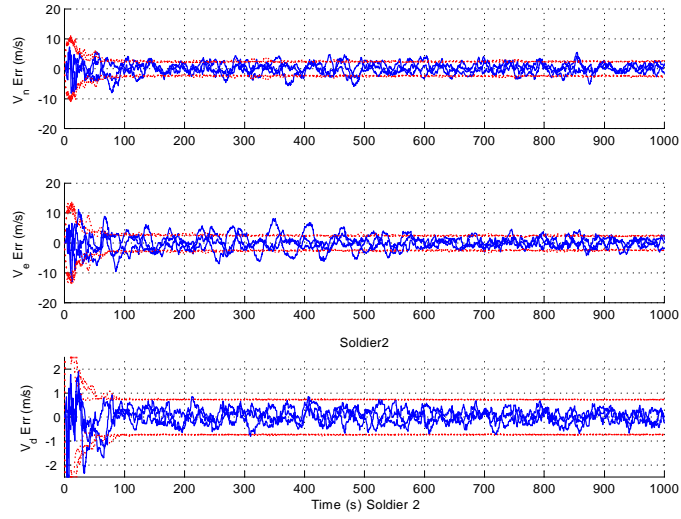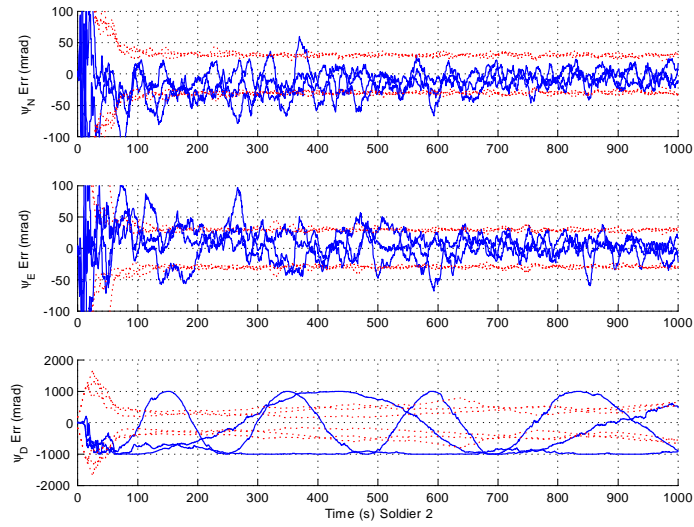
Figure 6.3: Test Scenario 1: Radio Only-2 Soldiers case, Soldier 1, Attitude Error in NED (Blue), Filter Calculated Error 2-σ (Red), 3 Monte-Carlo Runs
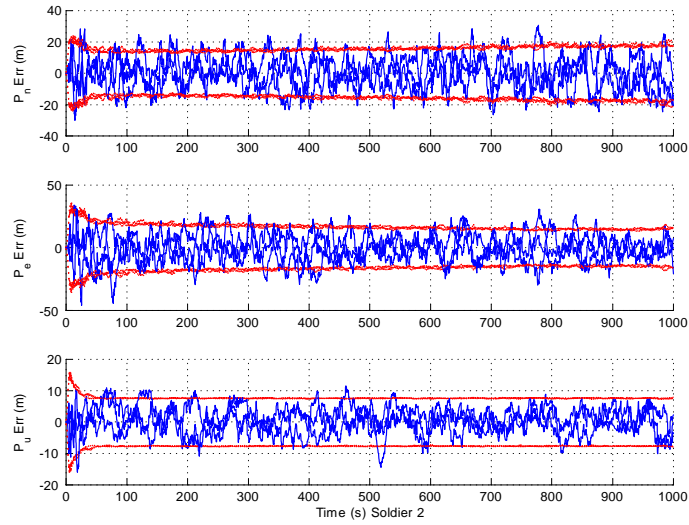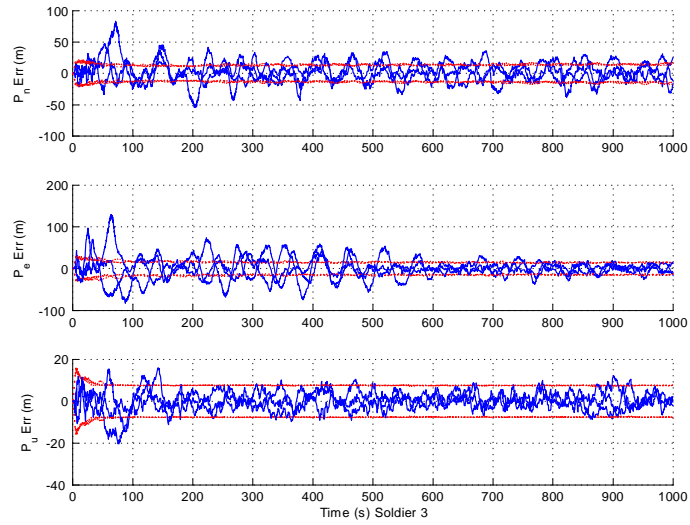

Figure 6.4: Test Scenario 1: Radio Only-2 Soldiers case, Soldier 2, Position Error in NED (Blue), Filter Calculated Error 2-σ (Red), 3 Monte-Carlo Runs
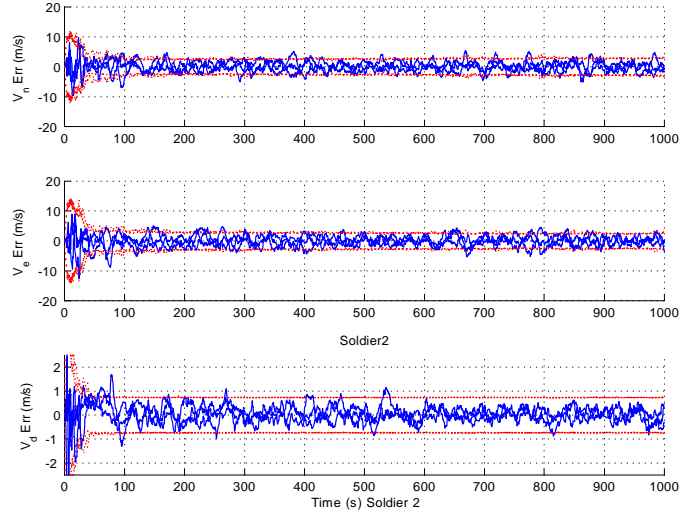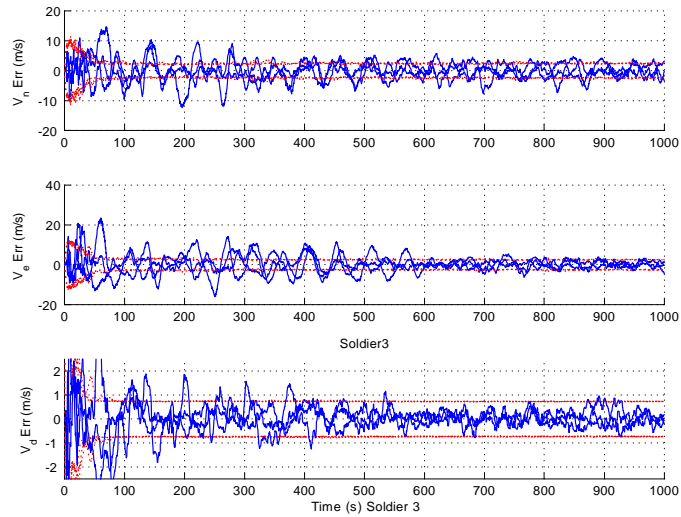
Figure 6.5: Test Scenario 1: Radio Only-2 Soldiers case, Soldier 2, Velocity Error in NED (Blue), Filter Calculated Error 2-σ (Red), 3 Monte-Carlo Runs
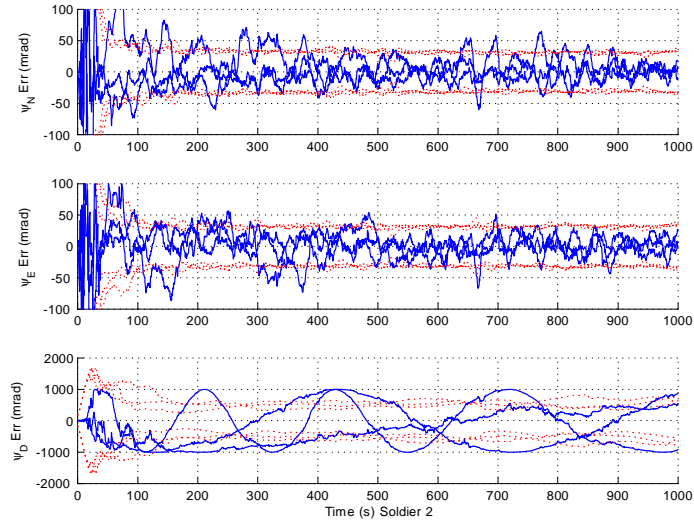
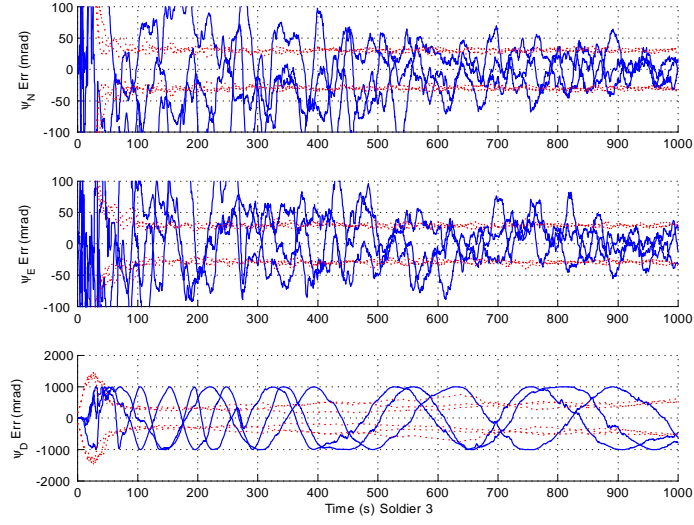Figure 6.6: Test Scenario 1: Radio Only-2 Soldiers case, Soldier 2, Attitude Error in NED (Blue), Filter Calculated Error 2-σ (Red), 3 Monte-Carlo Runs
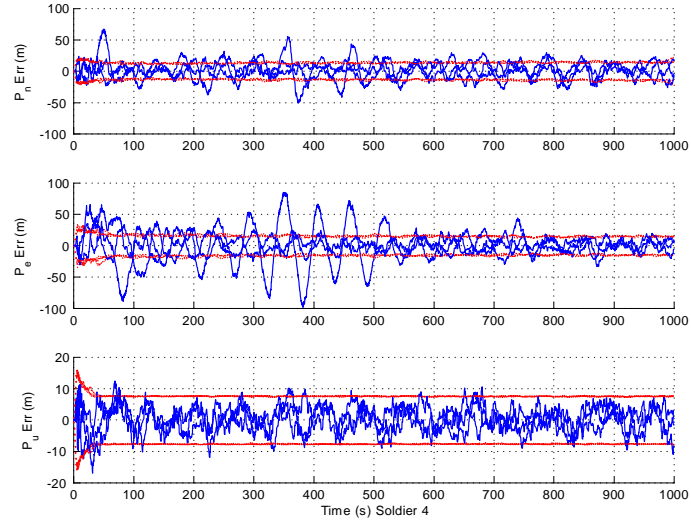
Test Scenario 2: Radio only, 4 Soldiers

Figure 6.7: Test Scenario 2: Radio Only-4 Soldiers case, Soldier 1, Position Error in NED (Blue), Filter Calculated Error 2-σ (Red), 3 Monte-Carlo Runs

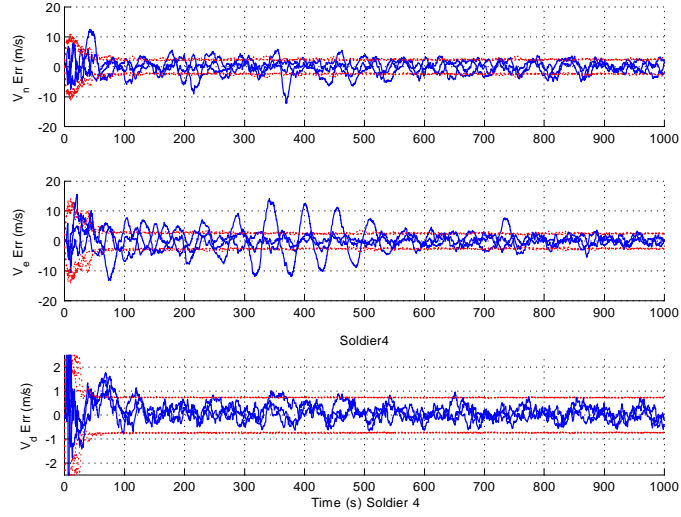Figure 6.8: Test Scenario 2: Radio Only-4 Soldiers case, Soldier 1, Velocity Error in NED (Blue), Filter Calculated Error 2-σ (Red), 3 Monte-Carlo Runs

Figure 6.9:   Test Scenario 2: Radio Only-4 Soldiers case, Soldier 1, Attitude error in NED (Blue), Filter Calculated Error 2-σ (Red), 3 Monte-Carlo Runs

Figure 6.10:   Test Scenario 2: Radio Only-4 Soldiers case, Soldier 2, Position Error in NED (Blue), Filter Calculated Error 2-σ (Red), 3 Monte-Carlo Runs

Figure 6.11: Test Scenario 2: Radio Only-4 Soldiers case, Soldier 2, Velocity Error in NED (Blue), Filter Calculated Error 2-σ (Red), 3 Monte-Carlo Runs
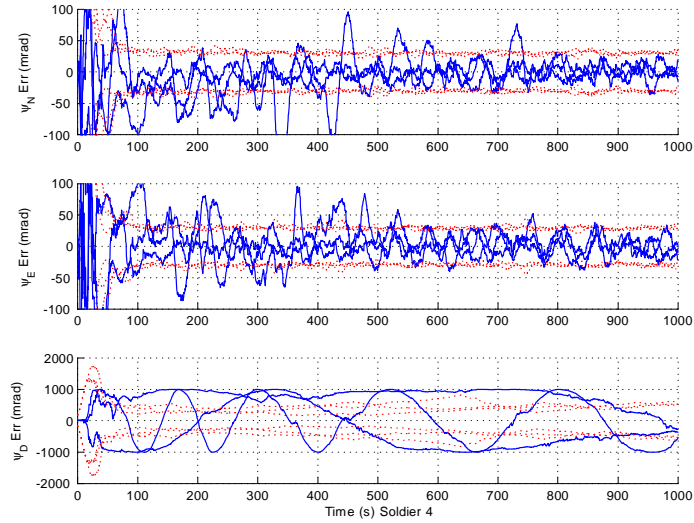

Figure 6.12: Test Scenario 2: Radio Only-4 Soldiers case, Soldier 2, Attitude Error in NED (Blue), Filter Calculated Error 2-σ (Red), 3 Monte-Carlo Runs
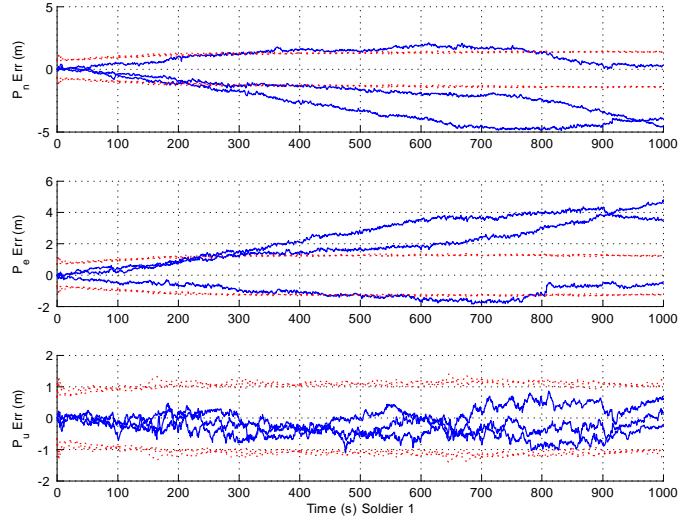
Figure 6.13: Test Scenario 2: Radio Only-4 Soldiers case, Soldier 3, Position Error in NED (Blue), Filter Calculated Error 2-σ (Red), 3 Monte-Carlo Runs

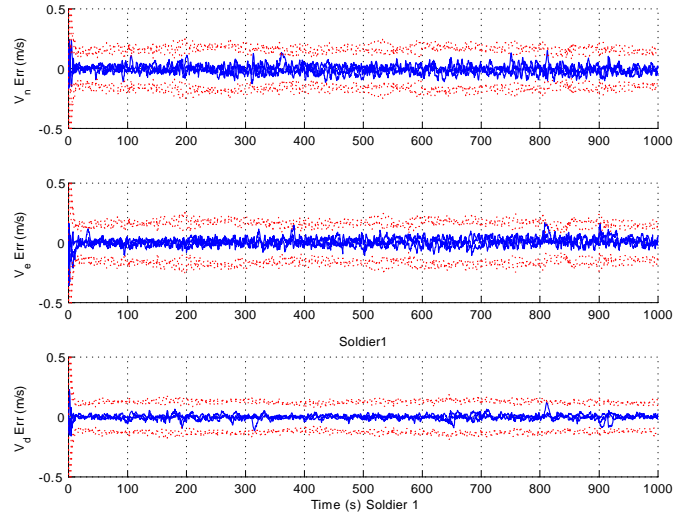Figure 6.14: Test Scenario 2: Radio Only-4 Soldiers case, Soldier 3, Velocity Error in NED (Blue), Filter Calculated Error 2-σ (Red), 3 Monte-Carlo Runs

Figure 6.15: Test Scenario 2: Radio Only-4 Soldiers case, Soldier 3, Attitude Error
in NED (Blue), Filter Calculated Error 2-σ (Red), 3 Monte-Carlo Runs

Figure 6.16: Test Scenario 2: Radio Only-4 Soldiers case, Soldier 4, Position Error
in NED (Blue), Filter Calculated Error 2-σ (Red), 3 Monte-Carlo Runs

6-8

Figure 6.17: Test Scenario 2: Radio Only-4 Soldiers case, Soldier 4, Velocity Error in NED (Blue), Filter Calculated Error 2-σ (Red), 3 Monte-Carlo Runs

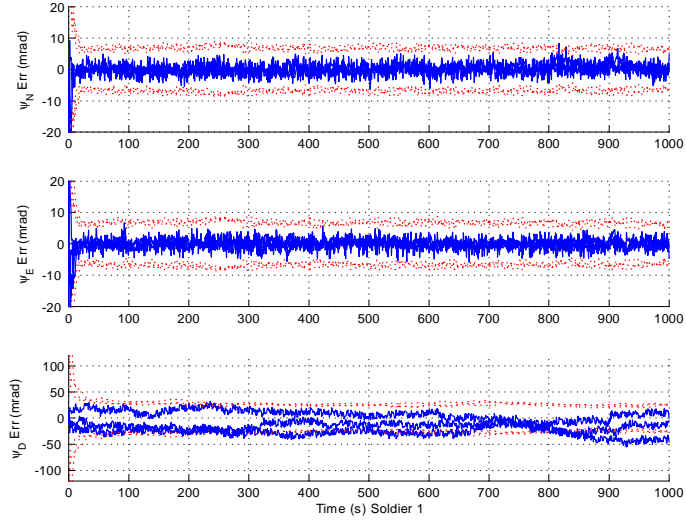Figure 6.18: Test Scenario 2: Radio Only-4 Soldiers case, Soldier 4, Attitude Error in NED (Blue), Filter Calculated Error 2-σ (Red), 3 Monte-Carlo Runs
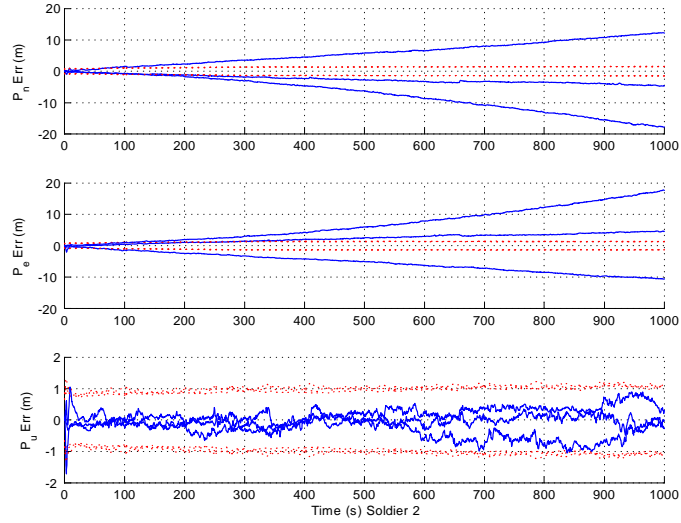
Test Scenario 3: Radio and Images, 2 Soldiers

Figure 6.19: Test Scenario 3: Radio and Image-2 Soldiers case, Soldier 1, Position Error in NED (Blue), Filter Calculated Error 2-σ (Red), 3 Monte-Carlo Runs
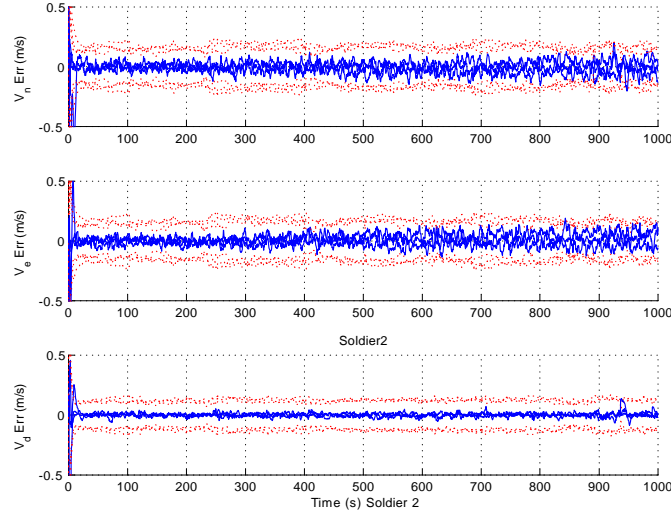

Figure 6.20: Test Scenario 3: Radio and Image-2 Soldiers case, Soldier 1, Velocity error in NED (Blue), Filter Calculated Error 2-σ (Red), 3 Monte-Carlo Runs
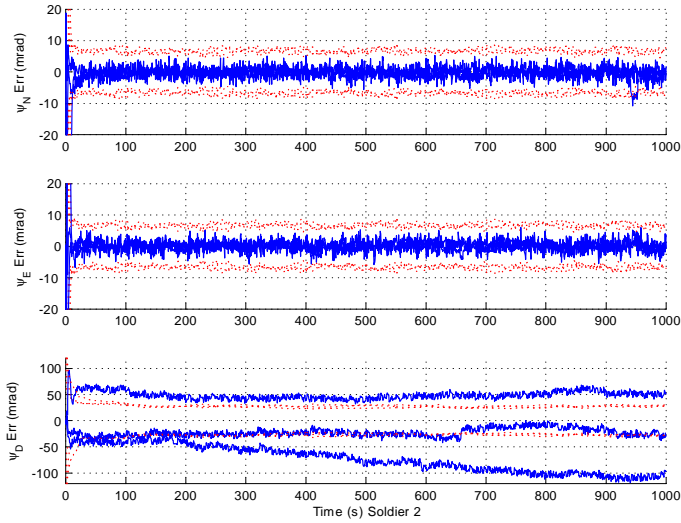
Figure 6.21:   Test Scenario 3: Radio and Image-2 Soldiers case, Soldier 1, Attitude Error in NED (Blue), Filter Calculated Error 2-σ (Red), 3 Monte-Carlo Runs

Figure 6.22:   Test Scenario 3: Radio and Image-2 Soldiers case, Soldier 2, Position Error in NED (Blue), Filter Calculated Error 2-σ (Red), 3 Monte-Carlo Runs

Figure 6.23: Test Scenario 3: Radio and Image-2 Soldiers case, Soldier 2, Velocity

Error in NED (Blue), Filter Calculated Error 2-σ (Red), 3 Monte-Carlo Runs

Figure 6.24: Test Scenario 3: Radio and Image-2 Soldiers case, Soldier 2, Attitude

error in NED (Blue), Filter Calculated Error 2-σ (Red), 3 Monte-Carlo Runs
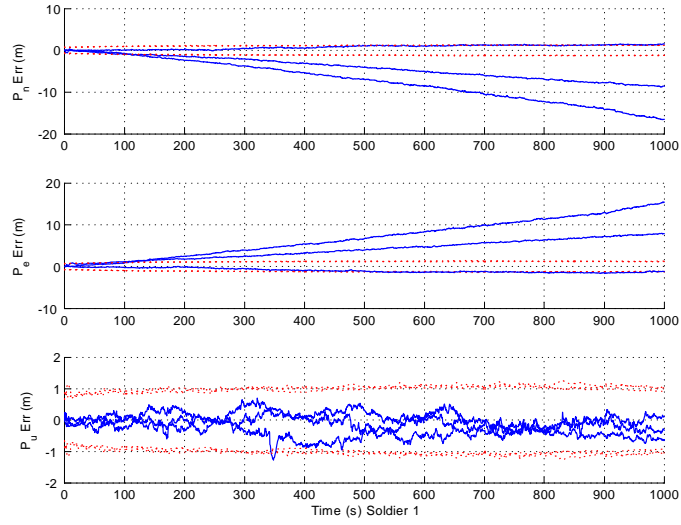
Test Scenario 4: Radio and Images, 4 Soldiers

Figure 6.25: Test Scenario 4: Radio and Image-4 Soldiers case, Soldier 1, Position Error in NED (Blue), Filter Calculated Error 2-σ (Red), 3 Monte-Carlo Runs

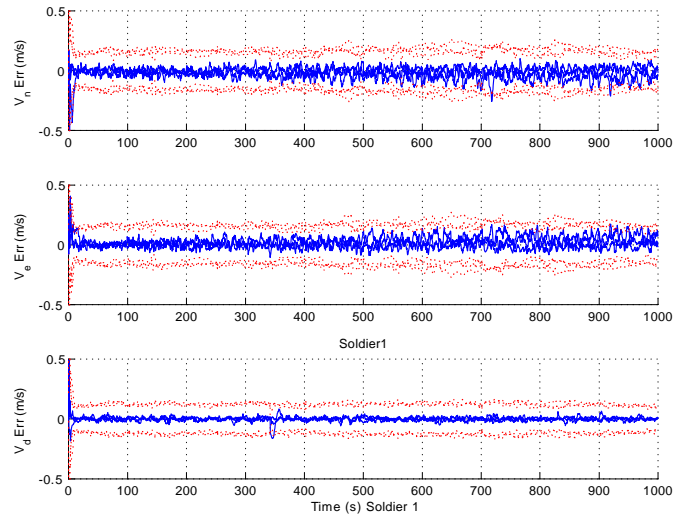Figure 6.26: Test Scenario 4: Radio and Image-4 Soldiers case, Soldier 1, Velocity Error in NED (Blue), Filter Calculated Error 2-σ (Red), 3 Monte-Carlo Runs
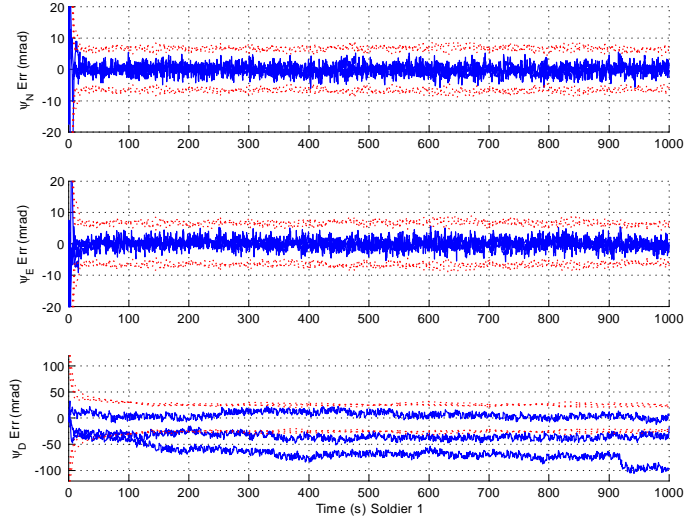
Figure 6.27:   Test Scenario 4: Radio and Image-4 Soldiers case, Soldier 1, Attitude Error in NED (Blue), Filter Calculated Error 2-σ (Red), 3 Monte-Carlo Runs

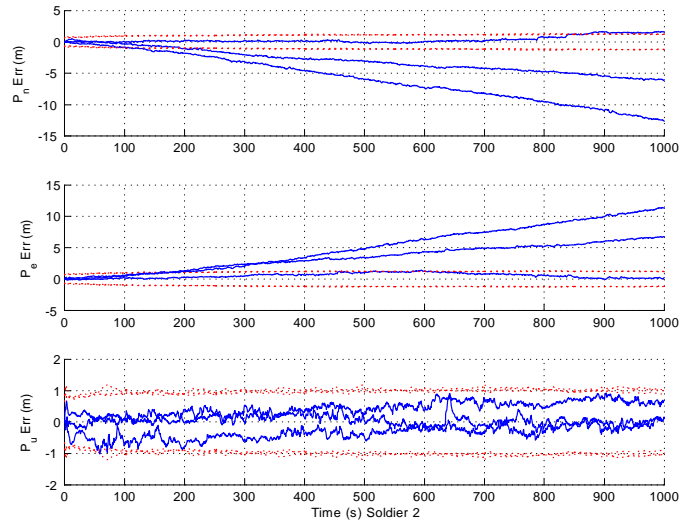Figure 6.28:   Test Scenario 4: Radio and Image-4 Soldiers case, Soldier 2, Position Error in NED (Blue), Filter Calculated Error 2-σ (Red), 3 Monte-Carlo Runs
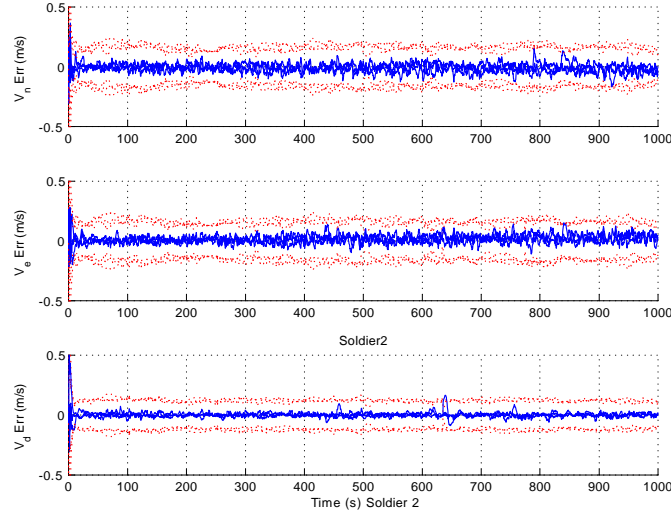
Figure 6.29: Test Scenario 4: Radio and Image-4 Soldiers case, Soldier 2, Velocity Error in NED (Blue), Filter Calculated Error 2-σ (Red), 3 Monte-Carlo Runs
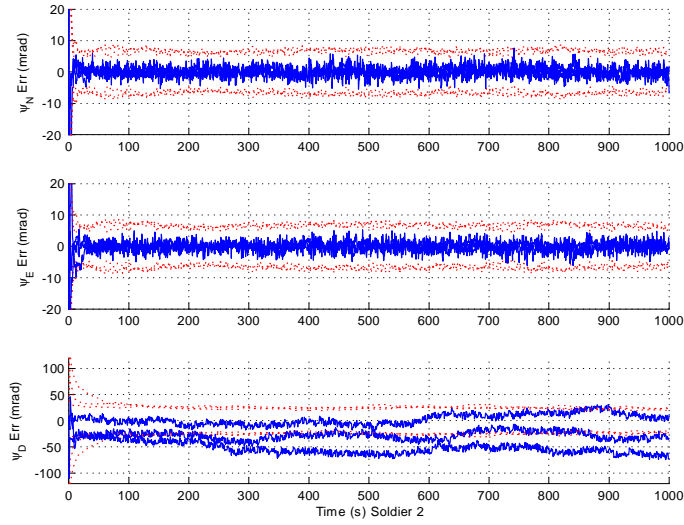

Figure 6.30: Test Scenario 4: Radio and Image-4 Soldiers case, Soldier 2, Attitude Error in NED (Blue), Filter Calculated Error 2-σ (Red), 3 Monte-Carlo Runs

Figure 6.31: Test Scenario 4: Radio and Image-4 Soldiers case, Soldier 3, Position
Error in NED (Blue), Filter Calculated Error 2-σ (Red), 3 Monte-Carlo Runs

Figure 6.32: Test Scenario 4: Radio and Image-4 Soldiers case, Soldier 3, Velocity
Error in NED (Blue), Filter Calculated Error 2-σ (Red), 3 Monte-Carlo Runs

Figure 6.33: Test Scenario 4: Radio and Image-4 Soldiers case, Soldier 3, Attitude Error in NED (Blue), Filter Calculated Error 2-σ (Red), 3 Monte-Carlo Runs
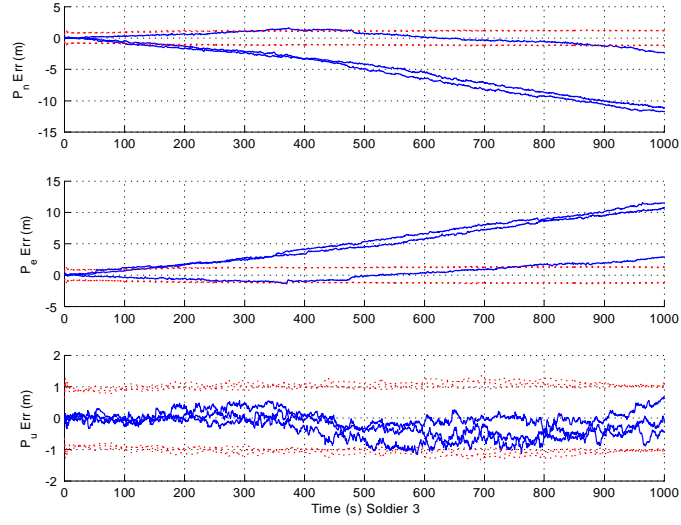

Figure 6.34: Test Scenario 4: Radio and Image-4 Soldiers case, Soldier 4, Position Error in NED (Blue), Filter Calculated Error 2-σ (Red), 3 Monte-Carlo Runs
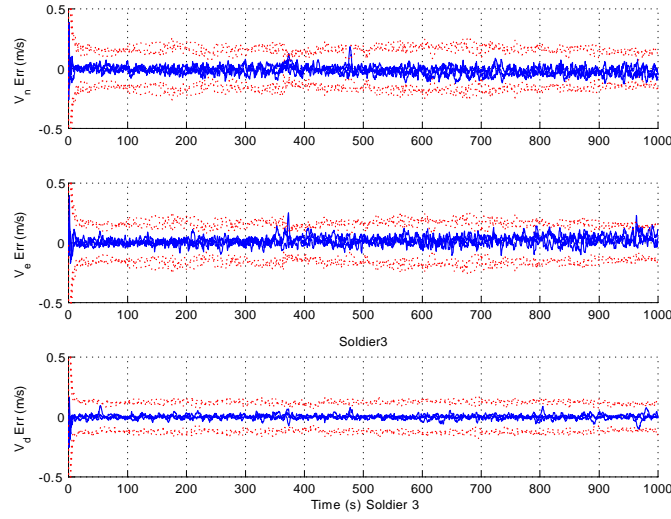
6-17

Figure 6.35: Test Scenario 4: Radio and Image-4 Soldiers case, Soldier 4, Velocity error in NED (Blue), Filter Calculated Error 2-σ (Red), 3 Monte-Carlo Runs

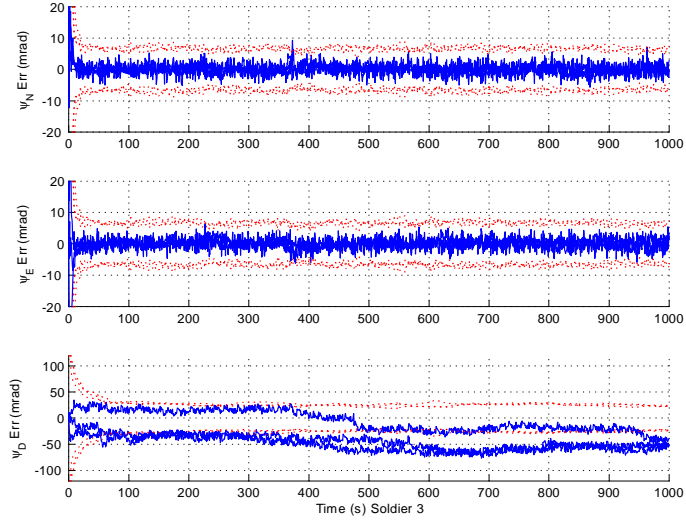Figure 6.36: Test Scenario 4: Radio and Image-4 Soldiers case, Soldier 4, Attitude Error in NED (Blue), Filter Calculated Error 2-σ (Red), 3 Monte-Carlo Runs
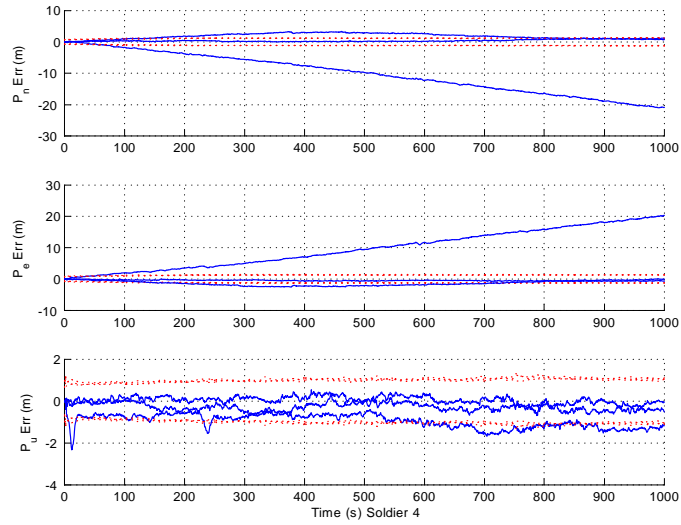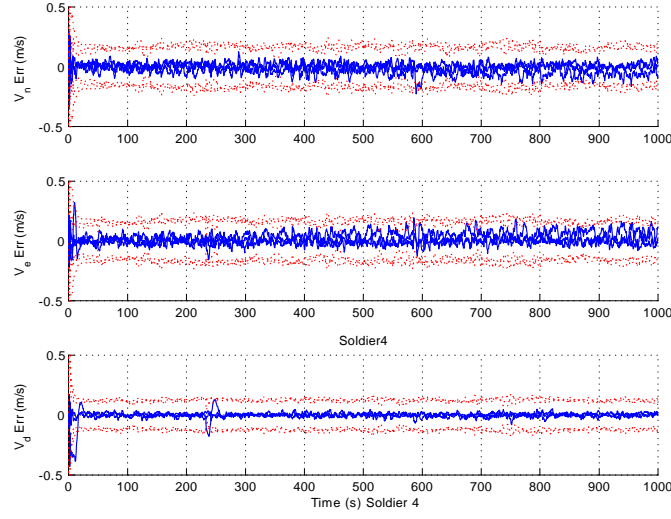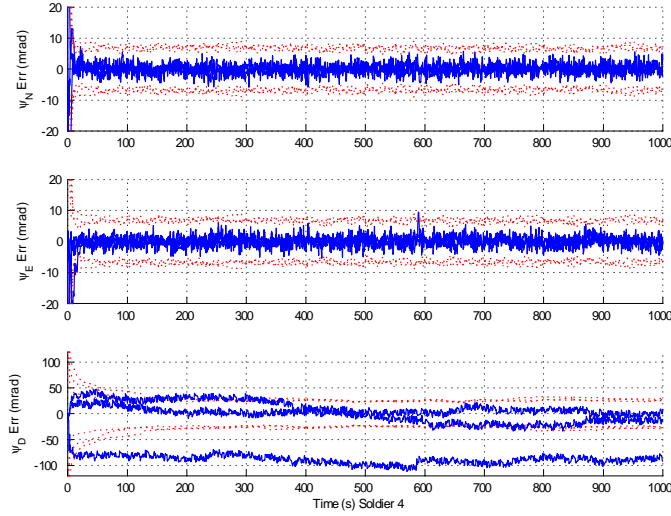
Bibliography

1. Bingham, Jason. *Vision-Aided, Cooperative Navigation For Multiple Unmanned Vehicles*. MS thesis, Air Force Institute of Technology, March 2009.

2. Brown, Robert and Patrick Wang. *Introduction to Random Signals and Applied Kalman Filtering*. New York, New York: John Wiley and Sons, 1997.

3. Jamie Morrisson, John Raquet, Michael Veth. "Performance Evaluation of Vision Aided Inertial Navigation System Augmented with a Coded Aperture.". January 2009.

4. Maybeck, Peter S. *Stochastic Models, Estimation, and Controls Volume 2*. New York, New York: Academic Press, 1982.

5. Maybeck, Peter S. *Stochastic Models, Estimation, and Controls Volume 1*. Arlington, Virginia: Navtech Book and Software Store, 1994.

6. National Imagery and Mapping Agency. *Department of Defense World Geodetic System 1984 - Its Definition and Relationships with Local Geodetic Systems*. Technical Report 8350.2, St. Louis, MO: Department of Computer Science, Michigan State University, January 2000.

7. Titterton, David and John Wston. *Strapdown Inertial Navigation Technology*. Herts. SGl 2AY, United Kingdom: The Institution of Electrical Engineers, 2004.

8. Veth, Michael. *Fusion of Imaging and Inertial Sensors for Navigation*. PhD dissertation, Air Force Institute of Technology, September 2006.

REPORT DOCUMENTATION PAGE

Form Approved
OMB No. 074-0188

The public reporting burden for this collection of information is estimated to average 1 hour per response, including the time for reviewing instructions, searching existing data sources, gathering and maintaining the data needed, and completing and reviewing the collection of information. Send comments regarding this burden estimate or any other aspect of the collection of information, including suggestions for reducing this burden to Department of Defense, Washington Headquarters Services, Directorate for Information Operations and Reports (0704-0188), 1215 Jefferson Davis Highway, Suite 1204, Arlington, VA 22202-4302. Respondents should be aware that notwithstanding any other provision of law, no person shall be subject to an penalty for failing to comply with a collection of information if it does not display a currently valid OMB control number.
PLEASE DO NOT RETURN YOUR FORM TO THE ABOVE ADDRESS.

1. REPORT DATE (DD-MM-YYYY) 26-03-2009	2. REPORT TYPE Master's Thesis	3. DATES COVERED (From – To) March 2008 - March 2009

4. TITLE AND SUBTITLE	5a. CONTRACT NUMBER
Performance Enhancements of Ranging Radio Aided Navigation	5b. GRANT NUMBER
	5c. PROGRAM ELEMENT NUMBER
6. AUTHOR(S)	5d. PROJECT NUMBER JON# 09-702
Ernsberger, Patirc J., Maj, USAF	5e. TASK NUMBER CRADA #08-AFIT-10
	5f. WORK UNIT NUMBER

7. PERFORMING ORGANIZATION NAMES(S) AND ADDRESS(S)	8. PERFORMING ORGANIZATION REPORT NUMBER
Air Force Institute of Technology Graduate School of Engineering and Management (AFIT/EN) 2950 Hobson Way WPAFB OH 45433-7765 DSN: 785-3636	AFIT/GE/ENG/09-15

9. SPONSORING/MONITORING AGENCY NAME(S) AND ADDRESS(ES)	10. SPONSOR/MONITOR'S ACRONYM(S)
Raytheon (CRADA #08-AFIT-10) Attn: Michael Fleenor 1801 Hughes Dr., Fullerton, CA 92833 mdfleenor@raytheon.com	11. SPONSOR/MONITOR'S REPORT NUMBER(S)

12. DISTRIBUTION/AVAILABILITY STATEMENT
Approval for public release; distribution is unlimited.

13. SUPPLEMENTARY NOTES

14. ABSTRACT

To accomplish Navigation in areas denied Global Navigation Satellite System (GNSS), such as around buildings or in steep valleys, alternative methods must be used. Radio ranging systems have been a part of the navigation solution for years. To improve the position estimate it is believed that using vision, consumer grade inertial navigation systems, and any other measurement available can aid the navigation solution. To accomplish this, an extended Kalman .filter was developed. It was configured as a centralized .filter. This produced the optimal solution showing that as image measurements were added, the navigation solution did improve. To simulate this with multiple vehicle and/or soldiers required a large state vector for the Kalman filter. To manage the large number of states and efficiently incorporate them into influence matrix's, a "Rosetta stone" was designed for state management.

15. SUBJECT TERMS
Radio Ranging, Image Aiding, Global Positioning System, Kalman Filtering, Inertial Navigation

16. SECURITY CLASSIFICATION OF:			17. LIMITATION OF ABSTRACT	18. NUMBER OF PAGES	19a. NAME OF RESPONSIBLE PERSON Raquet, John F., Ph.D., AFIT
REPORT U	ABSTRACT U	c. THIS PAGE U	UU	75	19b. TELEPHONE NUMBER (Include area code) (937) 255-3636, ext 4580 john.raquet@afit.edu

Standard Form 298 (Rev. 8-98)
Prescribed by ANSI Std. Z39.18